HEB collaborates with TCR signaling to upregulate *Id3* and enable γδT17 cell maturation in the fetal thymus

Johanna S. Selvaratnam[1,2], Juliana Dutra Barbosa da Rocha[1,2], Vinothkumar Rajan[1,2], Helen Wang[1,2], Emily C. Reddy[3], Jenny Jiahuan Liu[1,2], Miki S. Gams[2,3], Cornelis Murre[4], David L. Wiest[5], Cynthia J. Guidos[2,3], Juan Carlos Zúñiga-Pflücker[1,2], Michele K. Anderson[1,2]*

[1]Biological Sciences, Sunnybrook Research Institute, Toronto, ON, Canada

[2]Department of Immunology, University of Toronto, Toronto, ON, Canada

[3]Hospital for Sick Children, Toronto, ON, Canada

[4]Department of Molecular Biology, University of California at San Diego, La Jolla, CA, USA

[5]Blood Cell Development and Function Program, Fox Chase Cancer Center, Philadelphia, PA, USA

*Corresponding author: manderso@sri.utoronto.ca

Definitions of Acronyms and Abbreviations: TCR, T cell receptor; Id, Inhibitor of DNA binding; HEB, HeLa binding box transcription factor; IL, interleukin; E, embryonic day; V, variable region; Egr, early growth response; DP, $CD4^+CD8^+$ double positive thymocytes; DN, $CD4^-CD8^-$ double negative thymocytes; UMAP, uniform manifold approximation and projection for dimensional reduction; PCA, principal component analysis; sc, single cell; IFN, interferon

ABSTRACT

T cells expressing the γδ T cell receptor (TCR) develop in a stepwise process initiating at the αβ/γδ T cell lineage choice followed by maturation and acquisition of effector functions, including the ability to produce interleukin-17 (IL-17) as γδT17 cells. Previous studies linked TCR signal strength and T cell fate choices to the transcriptional regulator HEB (encoded by *Tcf12*) and its antagonist, Id3, but how these factors regulate different stages of γδ T cell development has not been determined. We found that immature fetal γδTCR$^+$ cells from conditional *Tcf12* knockout (HEB cKO) mice were defective in activating the γδT17 program at an early stage, whereas *Id3* deficient (Id3-KO) mice displayed a partial block in γδT17 maturation and an inability to produce IL-17. We also found that HEB cKO mice failed to upregulate *Id3* during γδT17 development, whereas HEB overexpression elevated the levels of *Id3* in collaboration with TCR signaling. Moreover, Egr2 and HEB were bound to several of the same regulatory sites on the *Id3* gene locus in the context of early T cell development. Therefore, our findings reveal an interlinked sequence of events during which HEB and TCR signaling synergize to upregulate *Id3*, which enables maturation and acquisition of the γδT17 effector program.

One Sentence Summary: The transcription factor HEB synergizes with TCR signaling to upregulate *Id3*, which is required for the maturation of fetal IL-17-producing γδ T cells.

INTRODUCTION

IL-17–producing γδ T (γδT17) cells are critical effectors in immune responses to bacterial and fungal pathogens and contribute to tissue repair and barrier integrity, particularly at mucosal surfaces (*1*). Beyond host defense, γδT17 cells regulate adipose tissue homeostasis and metabolic function (*2*). However, dysregulation of γδT17 cell function has been linked to autoimmunity and neuroinflammatory disorders, underscoring the importance of precisely controlled γδT17 cell development and function (*3, 4*).

While significant progress has been made in defining the stages of γδ T cell development, the transcriptional networks that govern lineage commitment and effector fate specification remain incompletely understood. In mice, γδT17 cells arise exclusively during fetal and early neonatal thymic development. The earliest wave of γδT17 cells in the fetal thymus, which emerges around embryonic day 17 (E17), originates from T cell precursors expressing the Vγ6 Vδ1 T cell receptor (TCR) (*5, 6*). A second wave of $V\gamma4^{+}V\delta5^{+}$ cells, which begins at E18, also gives rise to γδT17 cells (*7, 8*). By contrast, fetal-restricted $V\gamma5^{+}V\delta1^{+}$ γδ T cells are associated with the IFN-γ–producing γδT1 fate (*9, 10*). Most $V\gamma1^{+}$ cells, which appear just before birth and continue to develop in the adult thymus, also differentiate into γδT1 cells (*11*). Although $V\gamma4^{+}$ cells continue to be generated in the adult thymus, their capacity to give rise to innate γδT17 cells is significantly diminished (*7, 12, 13*). Instead, adult $V\gamma4^{+}$ cells remain poised for peripheral polarization into either γδT17 or γδT1 fates (*14*). Other subsets, such as IL-4 producing $V\gamma1^{+}V\delta6.3^{+}$ cells, emerge primarily in neonatal and young mice (*15*).

γδ and αβ T cells develop primarily from shared intrathymic T cell progenitors that lack expression of CD4 and CD8 (double-negative, DN) (*16, 17*). These precursors can be further subdivided by CD44 and CD25 expression, with the earliest thymic immigrants classified as $CD44^{+}CD25^{-}$,

termed early thymic progenitors (ETPs). In the fetal thymus, DN2 ($CD44^+CD25^+$) cells can generate either γδT17 or γδT1 cells, while DN3 ($CD44^-CD25^+$) cells preferentially give rise to γδT1 cells or proceed to αβ development following pre-TCR signaling in a process known as β-selection (*18*). Successful progress through β-selection is followed by upregulation of CD8 and CD4, generating $CD4^+CD8^+$ double positive (DP) cells. Commitment to the γδ lineage is initiated by γδTCR signaling, which induces lineage-specifying transcription factors such as *Sox13* (*19, 20*), followed by effector programming factors such as *Maf*, which are gradually upregulated as differentiation proceeds (*19, 21*). These factors promote expression of lineage-defining cytokines such as IL-17 and their regulators, including RORγt (*22*).

TCR signal strength plays a central role in determining both the γδ T cell lineage choice and γδ T cell effector program (*23, 24*). Weak pre-TCR signals promote αβ lineage progression, whereas intermediate γδTCR signaling favors γδT17 cell development, and stronger signals direct γδT1 differentiation (*25, 26*). Signal strength is modulated by TCR affinity, proximal CD3 signaling, and cytokine crosstalk (*27-30*). Together, these factors converge on downstream signal transduction pathways, including the ERK–Egr–Id3 axis, which has been identified as a key mediator of TCR signal strength using manipulation of TCR ligands or TCR signaling pathways (*10, 31-34*).

Id3 encodes a dominant-negative HLH protein that inhibits the expression of E protein-dependent genes. Id3 acts at the post-translational level by binding and sequestering E proteins, including HEB (encoded by *Tcf12*) and E2A (encoded by *Tcf3*), thereby preventing their DNA binding activity. HEB and E2A orchestrate multiple stages of αβ T cell development (*35-38*). *Id3* expression is proportional to TCR signal strength, suggesting that it may influence T cell fate by titrating E protein activity (*29, 39*). Moreover, Id3 is directly regulated by graded expression of

Egr factors, linking TCR signal strength to E protein target genes (*39*). We previously showed that HEB-deficient mice exhibit severe defects in γδT17 development, including impaired production of fetal Vγ4^{+} γδ T cells and dysregulated expression of key γδT17 regulators in the Vγ6^{+} subset (*8*). HEB directly activates early γδT17 genes, such as *Sox4* and *Sox13*, which are repressed when *Id3* is overexpressed. However, the complete physiological role of HEB in γδ T cell development remains unresolved.

Here, we investigated the roles of HEB and Id3 *in vivo* by analyzing fetal γδ T cell development in HEB$^{fl/fl}$;Vav-iCre (HEB conditional knockout, HEB cKO) and Id3-deficient (Id3-KO) mice using flow cytometry and single-cell RNA sequencing (scRNA-seq) of E18 thymocytes. Our results reveal a tiered disruption of γδ T cell development in HEB cKO mice, including dysregulated TRVG and TRDV expression, lineage diversion to the αβ program, and failure to activate key specification factors, including *Id3*. In contrast, γδT17 precursors in Id3-KO mice initiated the γδT17 specification program but failed to mature or produce IL-17. These findings suggest that HEB and Id3 function in an interlinked negative feedback loop that reinforces γδ lineage commitment and mediates the transition from specification to maturation during γδT17 cell development.

RESULTS

Strategy for analyzing γδ T cell developmental progression in the fetal thymus

To analyze γδ T cell development by flow cytometry, we used a panel of antibodies that distinguished developmental stages and lineage fate choices in the mouse fetal thymus. γδ T cells develop from DN2/3 cells in the thymus from precursors with both αβ and γδ T cell potential, with upregulation of CD8 (immature single positive, ISP) and CD4 marking commitment to the αβ-T cell lineage (**Fig. 1A**). Strong γδTCR signaling results in upregulation of CD73 (*Nt5e*), followed by downregulation of CD24 (*Cd24a*) to yield mature $CD27^{+}CD24^{-}CD73^{+}CD44^{-}$ γδT1 (IFNγ producing) cells. Signaling through $V\gamma6^{+}$ or $V\gamma4^{+}$ TCRs results in downregulation of CD24 as γδ T cell precursors differentiate into mature $CD27^{-}CD24^{-}CD73^{-}$ γδT17 (IL-17–producing) cells. CD27 is expressed on all immature γδ T cells and stays on in mature γδT1 cells but is downregulated during γδT17 maturation. Thus, detection of γδTCR, CD4, CD8, CD24, CD73, CD27, and Vγ chains, and the genes that encode them, provides a solid framework for analyzing the impact of gene perturbations on fetal γδ T cell development and maturation.

It is important to clarify the Vγ and Vδ chain nomenclature used in this study (**Fig. 1B**). Cell surface proteins detected in flow cytometry assays were classified using the Tonegawa nomenclature (*40*). When referring to genes or gene transcripts, the International Immunogenetics Information System (IMGT) nomenclature (*41*) was used, except in scRNA-seq figures where R-Seurat program output gene names from the Mouse Genome Informatics (MGI) site were preserved (*42*). The numbering is the same in all three systems except for Vδ1, which is equivalent to TRDV4 (IMTG) and Trdv4 (MGI).

HEB deficiency impairs Vγ4 cell development and inhibits functional maturation of γδT17 cells in the E18 fetal thymus

To investigate how HEB loss affects fetal γδ T cell development, we crossed $HEB^{fl/fl}$ mice with $HEB^{fl/fl}$;Vav-iCre mice to generate littermates without Cre (wildtype, WT) or with Cre (HEB cKO). HEB cKO mice lack HEB in all hematopoietic cells, as previously described (*8, 43*). At embryonic day 18 (E18), HEB cKO thymocytes showed reduced cellularity (**Fig. 1C**) and a developmental block at the ISP-to-DP transition (**Suppl. Fig. 1**), as previously reported in adult HEB-deficient mice (*44, 45*). Although γδ T cells were proportionally increased in HEB cKO mice (**Fig. 1D, E**), their absolute numbers were comparable to WT mice (**Fig. 1F**), indicating that the reduced cellularity was primarily due to loss of DP thymocytes.

We next analyzed Vγ chain subsets. HEB cKO mice exhibited a marked reduction in the frequency (**Fig. 1G, I**) and absolute numbers of $V\gamma4^+$ cells (**Fig. 1J**), and a corresponding increase in the other Vγ subsets (**Fig. 1G, H, I, J**). Immature ($CD24^+$) cells were more prevalent across all Vγ subsets in HEB cKO mice, except for $V\gamma4^+$ cells, which had not yet matured in either WT or HEB cKO mice (**Fig. 1K**). Furthermore, fetal HEB cKO γδ T cells showed a major impairment in IL-17 production (**Fig. 1L**), consistent with our prior fetal thymic organ culture (FTOC) results (*8*). These findings indicate that even in the intact E18 thymic environment, HEB is essential for γδT17 cell development.

Single-cell transcriptomic analysis reveals a role for HEB in establishing γδ T cell identity

To assess the transcriptomic impact of HEB deficiency, we performed single-cell RNA sequencing (scRNA-seq) on $\gamma\delta TCR^+$ thymocytes sorted from E18 WT and HEB cKO littermates. After quality control, we merged the datasets, excluded myeloid cells, and regressed out cell cycle genes using Seurat (*46*). Our analysis identified eight distinct clusters (numbered 0 to 7) visualized as a UMAP

(**Fig. 2A**). WT cells were enriched in clusters 2 and 4, while HEB cKO cells dominated clusters 0, 1, and 3. Clusters 5–7 showed a more balanced distribution (**Fig. 2B, C**). To annotate the clusters, we curated 90 γδ T cell subset-defining genes from prior studies (*13, 21, 47-51*) (**Suppl. Table 1**). The top 10 differentially expressed genes were used to generate a clustered dot plot (**Fig. 2D**), which we used to identify each cluster. We classified clusters 2 and 6 as early γδT cells (γδTe1, γδTe2), clusters 1 and 4 as γδT17 progenitors (γδT17p), cluster 0 as γδT1 progenitors (γδT1p), cluster 7 as mature γδT1 cells (γδT1), cluster 5 as mature γδT17 cells (γδT17), and cluster 3 as αβ lineage-like cells (αβT).

Quantification of WT and HEB cKO cells per cluster (**Fig. 2E**) revealed that the γδT17p clusters segregated by genotype into WT (γδT17pw) and HEB cKO (γδT17pk) cells. HEB cKO cells were also over-represented in the αβT cluster and under-represented in the γδTe1 cluster. An unbiased heatmap of the top 10 most differentially expressed genes across all clusters further validated our assigned identities, and revealed additional genes associated with these subsets (**Fig. 2F**). These findings suggest that the loss of HEB impairs the early γδ T cell program and allows diversion toward the αβ T cell lineage.

HEB deficiency suppresses TRDV5 expression and promotes TRDV4 expression

We next confirmed that WT and HEB cKO cells within each cluster represented equivalent developmental subsets (**Suppl. Fig. 2A**). All immature γδ T cell clusters expressed *Cd24a* and *Cd27*, while mature subsets lacked *Cd24a*. Among mature cells, only γδT1 cells expressed *Cd27* and *Nt5e* (CD73), whereas γδT17 cells were uniquely *Cd44*-positive, consistent with our assignments. We also analyzed TRGV and TRDV gene expression (**Suppl. Fig. 2B, C**). In WT cells, TRGV4 and TRDV5 were co-expressed in γδTe and γδT17p populations but were greatly diminished in HEB cKO cells. TRGV6 and TRGV5 transcripts were detectable

in γδTe subsets from HEB cKO mice, consistent with a delay in Vγ6$^+$ and Vγ5$^+$ γδ T cell maturation (Fig. 1K), whereas TRDV4 was expressed more broadly and at higher levels in all immature HEB cKO γδ T cell subsets relative to WT counterparts. These results indicate that HEB plays an important role in maintaining the subset-specific and magnitude of TRGV5 and TRDV4 expression during γδ T cell development.

HEB deficiency impairs early γδ T cell signatures and enhances αβ-T lineage features

To further define differences between WT and HEB cKO cells at the transcriptomic level, we constructed gene modules composed of suites of signature genes for the γδTe1, γδTe2, αβT, γδT17p, γδT17, γδT1p, and γδT1 subsets, derived from the analysis of merged WT and HEB cKO cells (**Fig. 2D, F**; see Methods). These modules were used to assign scores in WT (left) and HEB cKO (right) cells, which were visualized using split dot plots.

This analysis revealed a pronounced loss of the γδTe1 gene signature in HEB cKO cells (**Fig. 3A**) alongside a notable increase in the αβT signature (**Fig. 3B**). The γδTe2, γδT17p, and γδT17 gene signatures were also diminished in HEB cKO cells relative to WT, whereas the γδT1p signature was enriched. We also examined expression of individual genes that were diagnostic for γδ T cell subsets. In the γδTe1 and γδTe2 subsets of HEB cKO mice, *Sox13* and *Etv5* were reduced and *Cd8b1* and *Dgkeos* were elevated relative to their WT counterparts (**Fig. 3D**). In γδT17p cells, αβT-lineage genes were not detectable, but Sox13 and Etv5 were still lower in HEB cKO cells than WT cells, potentially decoupling the specification and commitment events. A less dramatic reduction in *Il1r1* was observed in HEB cKO γδT17 cells (**Fig. 3E**), and the levels of *Nrgn* and *Eomes* were similar in γδT1 lineage cells (**Fig. 3F**). These results suggest that the impact of HEB

deficiency at the transcriptomic level was more pronounced in early γδ T cell subsets than in mature γδ T cells.

HEB deficiency obstructs γδT17 progenitor development and dampens TCR signal strength

The γδT17p subset segregated into distinct clusters in WT and HEB cKO cells, highlighting a critical stage of HEB-dependent regulation. To explore this further, we performed an unbiased differential gene expression analysis in WT cells versus HEB cKO cells and visualized the results using an enhanced volcano plot with stringent thresholds ($\log_2 FC > 0.5$, $-\log_{10} P > 25$) (**Fig. 4A**). Many of the top differentially expressed genes were signature markers of γδT17 differentiation, including *Blk, Sox13*, and *Etv5*, all of which were downregulated in HEB cKO cells. *Trdv4* was among the most upregulated genes in HEB cKO γδT17p cells.

We next generated a list of differentially expressed genes between WT and HEB cKO γδT17p cells using less stringent criteria (adj P value > 0.001, log2Fc > 0.25) (**Suppl. Table 2**). This list was subjected to gene ontology analysis using ShinyGO, which resulted in a list of KEGG pathways with reduced gene representation in HEB cKO γδT17p cells. We observed significant depletion of genes pathways related to TCR signaling (T cell receptor signaling, PD-1 checkpoint, NF-κB signaling) and Th1, Th2, and Th17 differentiation in HEB cKO cells relative to WT cells (**Fig. 4B**; **Suppl. Table 3**). Three key markers of TCR signal strength, *Cd5*, *Cd69*, and *Egr1*, were reduced in both γδTe2 and γδT17p subsets in HEB cKO mice (**Fig. 4C**). *Id3* expression was markedly decreased in HEB cKO γδTe cells and nearly absent in γδT17p cells but remained intact in γδT1p and γδT1 cells (**Fig. 4D, E**). We also examined the expression *Maf* and *Rorc*, two key regulators of γδT17 maturation, and found that they were expressed similarly between HEB cKO

and WT cells in each cluster (**Fig. 4F**). Therefore, HEB modulates TCR signaling during γδT17 specification but appears to be dispensable for the expression of γδT17 cell maturation factors.

Id3 expression in γδT17 progenitors is controlled through HEB-dependent mechanisms

To further elucidate the landscape of E protein and Id protein expression during γδ T cell development, we examined the expression of *Tcf12* (encodes HEB), *Tcf3* (encodes E2A), *Id3*, and *Id2* in each cluster (**Suppl. Fig. 3**). It should be noted that the *Tcf12* deletion occurs in one of the last exons of a 200 kb gene locus, and although the protein is absent (*44*), some mRNA expression can still be detected. In WT mice, γδTe cells co-expressed *Tcf12*, *Tcf3*, and *Id3* (**Suppl. Fig. 3A-C, E**), consistent with dynamic regulation of E protein-dependent target genes expression during the αβ/γδ fate choice (*52*). γδT17p cells co-expressed *Tcf12* and *Tcf3*, whereas γδT1 cells co-expressed *Tcf3* and *Id3* (**Suppl. Fig. 3B, D**). *Id2* expression was restricted to mature γδT17 and mature γδT1 cells in both WT and HEB cKO mice. *Tcf3* expression was also unaffected by a lack of HEB, indicating that *Tcf3* and *Id2* expression are HEB-independent (**Suppl. Fig. 3E, F**). *Id3* expression was disrupted in HEB cKO cells in γδTe and γδT17 cells but not in γδT1p cells (**Suppl. Fig. 3C, D)**. This analysis reveals that *Id3* expression was disrupted only in cells that normally express *Tcf12*.

Loss of *Id3* impairs CD73 upregulation and γδT17 cell function in the fetal thymus

Given the clear dependence of *Id3* expression on HEB in specific γδ T cell subsets, we next investigated how loss of *Id3* itself affects γδ T cell development using E18 fetal thymocytes from Id3 knockout (Id3-KO) mice. Total thymic cellularity in Id3-KO mice was comparable to WT controls (**Fig. 5A**), but the proportion of γδ T cells among total thymocytes was reduced (**Fig. 5B, C**). Analysis of Vγ chain usage revealed no major differences between WT and Id3-KO mice,

although there was a slight increase in the proportion of Vγ6$^+$ cells in Id3-KO γδ T cells (**Fig. 5F**). Interestingly, very few Id3-KO γδ T cells expressed CD73 (encoded by *Nt5e*) (**Fig. 5G, H**), including Vγ5$^+$ and Vγ1$^+$ cells (**Suppl. Fig. 4**). *Nt5e* expression is upregulated in response to strong TCR signaling during γδ T cell development, and it can also be induced in response to short-term stimulation (*53, 54*). To determine whether the deficiency in CD73 expression in Id3-KO mice reflected an expansion of CD73$^-$ cells or a failure to induce *Nt5e*, we cultured E18 fetal thymocytes from WT and Id3-KO mice with PMA/ionomycin (P/I) for four hours and measured CD73 expression in γδ T cells by flow cytometry. While CD73 was robustly induced in a substantial fraction of CD27$^+$ γδ T cells from WT mice, it remained nearly undetectable in Id3-KO γδ T cells (**Fig. 5I, J**), indicating a direct role for Id3 in the regulation of *Nt5e* expression.

Mature CD73$^-$ γδ T cells typically exhibit a bias toward the γδT17 lineage (*8*). We hypothesized that loss of *Id3* might re-direct γδT1-fated cells into the γδT17 lineage. However, upon stimulation, Id3-KO γδ T cells failed to produce IL-17 (**Fig. 5K, L**), indicating that *Id3* deficiency does not promote γδT17 differentiation. These findings highlight a critical role for *Id3* in the functional maturation of both CD73$^+$ and CD73$^-$ γδ T cells.

Loss of *Id3* disrupts expression of γδT17 cell maturation transcription factors

To further investigate how *Id3* deficiency affects γδ T cell development, we measured intracellular expression of PLZF (encoded by *Zbtb16*) and MAF in E18 γδ T cells from WT and Id3-KO mice by flow cytometry (**Fig. 6**). PLZF is expressed in innate fetal/neonatal γδ T cells and adult iNKT and IL-4–producing γδ T cells (*55-57*). To compare developmental stages within Vγ subsets between WT and Id3-KO γδ T cells, we gated on: 1) immature (CD24$^+$) Vγ4 cells, which comprised the majority of Vγ4 cells, 2) immature (CD24$^+$) Vγ6 cells, and 3) mature (CD24$^-$) Vγ6

cells (**Fig. 6A**). This analysis yielded three populations, based on PLZF and MAF expression: $PLZF^{+}MAF^{+}$, $PLZF^{+}MAF^{-}$, and $PLZF^{-}MAF^{-}$ cells (**Fig. 6B**).

In WT mice, most immature Vγ4 and Vγ6 cells expressed PLZF, with about half of the $PLZF^{+}$ cells co-expressing MAF. Nearly all mature Vγ6 cells co-expressed PLZF and MAF. Immature Vγ4 and Vγ6 subsets in Id3-KO mice had reduced proportions of $PLZF^{+}MAF^{+}$ cell proportions and increased percentages of $PLZF^{-}MAF^{-}$ cells relative to WT. Mature Vγ6 cells in Id3-KO mice exhibited a more severe disruption, with only ~50% co-expressing PLZF and MAF, and significant increases within the $PLZF^{+}MAF^{-}$ or $PLZF^{-}MAF^{-}$ subsets. Mean fluorescence intensity analysis revealed substantially lower PLZF protein levels in Id3-KO cells across all subsets, especially immature cells, suggesting that this defect is not solely due to delayed maturation (**Fig. 6C**).

Id3 deficiency promotes the αβ-T lineage but does not disrupt the expression of early γδ T cell regulators

To investigate population dynamics and gene expression changes in Id3-KO fetal thymocytes, we performed scRNA-seq on $CD4^{-}CD8^{-}$ E18 fetal thymocytes. This strategy was designed to capture γδ T-biased cells with low surface γδTCR that might be missed by flow cytometric cell sorting. After quality control, WT and Id3-KO datasets were merged and subjected to dimensionality reduction, which identified eleven clusters (0–10) (**Suppl. Fig. 5**). Violin plots of lineage and subset-specific genes identified two γδ T cell clusters, which were computationally isolated and reclustered. This process yielded four new γδ T cell clusters (0-3), which we identified as γδTe, γδT17p, γδT17, and γδT1 cells (**Fig. 6D, E**), using the same strategy shown in Fig. 2 (**Fig. 6G**). This scRNA-seq dataset lacked a γδ/αβ T lineage cluster, likely due to low cell numbers and/or exclusion of $CD4^{+}$ and $CD8^{+}$ cells in the enrichment strategy. However, flow cytometry of E18 fetal thymocytes revealed a significantly higher proportion of $TCR\gamma\delta^{+}$ cells co-expressing CD4

and CD8 in Id3-KO mice than in WT mice, indicating a bias toward the αβ T cell program (**Suppl. Fig. 6**). Notably, our scRNA-seq analysis showed that γδ T cell specification genes (*Sox13*, *Etv5*) and *Tcf12* were unaffected by the decrease in *Id3* (**Fig. 6H**). These results decouple the loss of *Id3* from the disruption of early γδ T cell regulators in HEB cKO mice.

Id3 is required for the induction of γδT17 regulators at the transcriptional level

Compared to WT, the Id3-KO mice had increased numbers of γδT17p cells and fewer mature γδT17 cells (**Fig. 6F**), consistent with a partial block in γδT17 maturation. *Id2* expression was markedly increased in all Id3-KO γδ T cell subsets (**Fig. 6I**), consistent with a previously reported compensatory role (*58*). *Maf* and *Zbtb16* transcripts were markedly reduced in Id3-KO cells at the γδTe stage but recovered to near WT levels in mature γδT17 cells (**Fig. 6I**). We noted a similar impact on expression of *Rora* in Id3-KO mice. *Rora* is not required for γδT17 cell function (*59*), but does play roles in regulation the development of Th17 (*60*) and ILC3 cells (*61*). We also examined expression of *Rorc* (encodes RORγt). Given the decrease in other genes involved in γδT17 cell maturation, and the dependence of *Rorc* expression on MAF in γδT17 cells (*22*), we were surprised to find that *Rorc* was higher in Id3-KO γδT17p cells than in WT γδT17p cells (**Suppl. Fig. 5D**) and was also elevated in the CD8-expressing DN4 subset (**Suppl. Fig. 5E**). Although RORγt is a critical regulator of γδT17 development and function, it is also upregulated after β-selection and maintains DP cell survival (*62*), suggesting that the increase we observed in the γδT17p cells could in part be due to αβ-T cell lineage diversion.

ChIP-Seq analysis reveals shared HEB, E2A, and Egr2 binding sites in the *Id3* locus

Although our data showed that HEB is necessary for *Id3* expression during γδT17 development, it remained unclear whether HEB directly regulates *Id3*. The *Id3* gene locus is composed of three

exons adjacent to the long non-coding RNA gene *Gm42329*, which lies in the opposite (tail-to-tail) orientation (**Fig. 7A**). To assess direct binding of HEB and/or E2A to the *Id3* locus, we analyzed ChIP-seq datasets from *Rag2*$^{-/-}$ DN3 thymocytes (*63*). This analysis identified three major binding regions for both HEB and E2A upstream of the first exon of *Id3*, each containing multiple peaks.

We also examined ChIP-seq datasets from DN3 cells stimulated with anti-CD3 or anti-TCRβ to mimic TCR signaling (*64, 65*). RNA polymerase II bound the *Id3* promoter in Rag2$^{-/-}$ mice stimulated with anti-CD3ε, revealing active *Id3* transcription in cells that had experienced CD3-mediated signaling. Additionally, we observed Egr2 binding to two sites that overlapped with the HEB/E2A regions in total thymocytes from mice that had been injected with anti-TCRβ (*64*). Notably, H3K27me3 repressive marks were detected across the *Gm42329* locus but were absent from *Id3*, indicating that *Id3* is epigenetically poised for activation before pre-TCR and/or γδTCR signaling occurs.

Together, these data suggest that *Id3* is a direct transcriptional target of HEB and E2A and that its induction in response to TCR signaling depends on the combined action of HEB, E2A, and Egr2 during the DN3 to DN4 transition.

TCR Signaling and HEB Converge to Potentiate *Id3* Transcription

To test whether HEB can cooperate with TCR/CD3 signaling to upregulate *Id3*, we used a gain-of-function approach. We took advantage of the SCID.adh cell line, which ectopically expresses a chimeric hIL-2Rα:CD3ε receptor that mimics pre-TCR signaling when stimulated with anti-TAC (hIL-2Rα) antibody (*66*). Stimulation results in downregulation of CD25, *Rag1*, *Rag2*, and *Ptcra*, while inducing *Trac* germline transcripts, recapitulating pre-TCR activity.

We transduced SCID.adh cells with either control or HEB-expressing retroviruses to generate control and HEB-overexpressing cells (**Fig. 7B**). To avoid the growth arrest and cell death associated with full-length HEB (HEBCan) overexpression (*67, 68*), we used HEBAlt, a truncated form that activates E protein target genes without impairing cell viability (*68-70*).

Upon overnight stimulation with anti-TAC, both control and HEB-expressing cells downregulated CD25 to similar degrees, as assessed by flow cytometry, confirming effective CD3-mediated signaling (**Fig. 7C, E**). Quantitative RT-PCR analysis showed that *Id3* expression was modestly elevated in unstimulated HEB-expressing cells compared to controls, and stimulation of control cells upregulated *Id3* levels to a greater degree (**Fig. 7D**). Notably, *Id3* expression in stimulated cells expressing HEB was much higher than either HEB or stimulation alone, and exceeded the sum of these two conditions, indicating a synergistic interaction.

These results demonstrate that HEB can amplify *Id3* induction in response to TCR signaling, likely through cooperative interaction with TCR-induced factors such as Egr2.

DISCUSSION

HEB and Id3 are both critical for T cell development, but their distinct functions in fetal γδ T cell development have not been resolved. Here, we show that HEB controls expression of genes involved in γδTCR signaling and induces a transcriptional program that primes γδ T cell precursors for γδT17 differentiation. Furthermore, HEB collaborates with TCR-dependent factors such as Egr2 to upregulate *Id3*, which enables γδT17 cell maturation and inhibits the αβ T cell fate. Together, these findings define a sequence of regulatory states governed by the E/Id axis that orchestrate γδ T cell lineage commitment and the differentiation of functional γδT17 cells.

TCR signal strength is tightly linked to specific combinations of Vγ and Vδ chains expressed on fetal γδ T cells, which serve as critical drivers of γδ T cell fate and functional programming (*12, 32, 34, 71*). We found that HEB is required for expression of TRGV4 and TRDV5. These genes encode the $V\gamma4^{+}V\delta5^{+}$ TCR, which supports γδT17 cell differentiation (*72*). While TRGV4 is known to be regulated by E proteins (*8, 73, 74*), the requirement for HEB in TRDV5 expression is newly appreciated. Notably, the TRD locus contains E2A-dependent insulators that limit TRDV4 expression to the fetal thymus (*75*). Whether these are also HEB-dependent, and whether they impact TRDV expression among fetal γδ T cell subsets, remains to be determined.

Our analysis identified known E protein target genes, including components of the TCR signaling pathway (*Cd3d*, *Cd3g*, *Lat*, *Zap70*) (*76, 77*) and chemokine receptors (*Cxcr5*, *Cxcr4*, *Ccr9*) (*78*), validating the experimental approach. Moreover, we found that a suite of γδT17-specific genes were also HEB-dependent, including *Blk* and *Syk*, which are γδT17 cell-specific mediators of TCR signaling. We also noted that several inhibitors of TCR signaling were decreased, including *Pdcd1* (encodes PD-1), *Nfbia* (encodes Ikappaα), and *Sh2d2a* (encodes TSAd). All of these inhibitors are

regulated post-translationally, suggesting a role for HEB in inducing T-lineage specific pathways that enable both positive and negative regulation of TCR signal transduction.

Our studies show that Id3 limits αβ-lineage potential even in the presence of HEB, suggesting that HEB restricts the αβ program primarily by upregulating *Id3*. In contrast, the early γδ T cell program is upregulated in Id3-KO mice, indicating that *Id3* is not required for this function. A third E/Id dynamic operates during γδT17 maturation, which requires *Id3* independently of HEB. Sox13 has been shown to initiate a cascade of regulatory events that induce *Blk* and *Maf* during γδT17 development (*8, 21*). However, our work indicates that Sox13 is not sufficient to upregulate γδT17 maturation factors like *Zbtb16* and *Maf* in the absence of *Id3*, implying an E-protein dependent brake on γδT17 maturation. This highlights a decoupling between lineage specification and effector maturation, supporting the two-step model of γδ T cell development (*54*).

Intriguingly, our results show that γδT1 lineage cells express *Tcf3* (E2A) but not *Tcf12* (HEB), consistent with an HEB-independent γδT1 gene regulatory network. It is possible that Id3 is needed after gd T cell specification to inhibit E2A-driven inhibitors of γδT17 maturation. Possible candidates include positive regulators of γδT1 differentiation, such as T-bet (*Tbx21*) or Eomes. These transcription factors participate in negative cross-regulatory loops with γδT17 regulators such as Runx1, RORγt, and AP-1 factors, which help to stabilize γδ T cell subset lineage identity (*79*). Additionally, transiently expressed HEB-dependent transcription factors such as *Etv5* and *Sox5* may act as a checkpoint for γδT17 maturation, to be released upon *Id3* upregulation.

The TCR signal strength model posits that strong signals induce high levels of Egr factors, which induce high levels of *Id3* (*25, 39*). Our data add an important new dimension to this paradigm, proposing that the lower Egr2 levels induced by weaker γδTCR signaling require cooperation with

HEB/E2A to upregulate *Id3* expression (**Suppl. Fig. 7A**). This model is supported by our ChIP-seq data, which confirms HEB and E2A binding at the *Id3* locus, at sites also bound by Egr2, and gain-of-function studies, which show that HEB synergizes with TCR/CD3 signals to amplify *Id3* expression. Both HEB and E2A are pioneering factors, and can increase locus accessibility of genes involved in lymphoid development, such as *Foxo1* (*43*). Therefore, HEB and E2A may epigenetically prime the *Id3* locus prior to TCR signaling.

Our data is consistent with a partial compensation for Id3 by Id2, less effectively during γδ T cell commitment, and more fully during late γδT17 maturation, when *Id2* is normally expressed. This is consistent with the observation that Id3 supports transient developmental transitions, while Id2 stabilizes innate-like transcriptional states (*80*). Since *Id2* is a direct target of E2A (*81*), the upregulation of *Id2* in *Id3*-deficient precursors likely reflects increased E protein activity. Thus, HEB, Id3, and Id2 participate in negative regulatory loops that allow transient HEB activity and Id3 expression, followed by stabilization of the innate γδT17 gene network by Id2 (**Suppl. Fig. 7B**). Understanding how Id3 and Id2 differentially regulate the timing and magnitude of E protein activity, and whether they have different impacts on E2A/E2A homodimers versus HEB/E2A heterodimers remains to be addressed.

There are limitations to our study. Our analyses focused on E18 γδ T cells, which reflect γδT17-biased fetal development and may not capture functions of HEB or Id3 at other stages. It is also unclear whether diminished PLZF and MAF expression reflects a cause or consequence of inhibited maturation. The specific contributions of HEBAlt and HEBCan isoforms remain unresolved, as both were deleted in our conditional HEB model. In addition, we have not yet addressed the roles of HEB and Id3 in TCR-independent development of a subset of fetal-derived $V\gamma4^{+}$ γδ T cells (*48*).

In summary, our studies have identified multiple interlinked transcriptional circuits that require E proteins and Id factors during γδ T cell development. HEB induces Id3, which then inhibits E protein activity. In the absence of Id3, HEB and E2A activity persist, inducing compensatory Id2 expression. Since Id3 expression is self-limiting through E protein suppression, the HEB-Id3 interactions result in a negative feedback loop. Thus, HEB plays dual roles in establishing γδ lineage identity and initiating γδT17 differentiation via Id3. Future work should clarify the direct transcriptional targets and co-factors of HEB, as well as how dynamic levels of HEB, Id3, and Id2 coordinate γδ T cell fate decisions.

MATERIALS AND METHODS

Experimental Design and Statistical Analysis

The overall goal of this study was to understand how HEB transcription factors regulate the transcriptional networks required for the development of IL-17 producing γδ T cells. The subjects of these studies were genetically modified mice. The experimental variable was the genotype of the mice, chosen based on availability of animals and littermate controls. For the scRNA-seq experiments, fetal thymocytes of like genotype from 3 or more mice were pooled prior to enrichment. Each flow cytometry analysis was performed using 3 or more mice of like genotype per experiment, repeated 2-3 times. Mice of both sexes were used. No sex differences were apparent; therefore, data were pooled. Each data point depicted in graphs represents an individual mouse. The investigators were not blinded to allocation during experiments and outcome assessment, except when fetal thymocytes were individually analyzed by flow cytometry prior to genotyping. Significance of pairwise data was computed by unpaired two-tailed Student's t-test, with $p < 0.05$ considered statistically significance. The error bars represent standard error of the mean (SEM) values.

Mice

$HEB^{fl/fl}$ mice have loxP sites flanking exons that encode the bHLH DNA binding and dimerization domain, which is shared by all HEB isoforms (*45, 69*). These mice were bred to Vav-iCre transgenic mice (JAX stock #008610) (*82*), which deletes regions flanked by loxP sites in all hematopoietic cells (*83*), to generate $HEB^{fl/fl;Vav\text{-}iCre}$ (HEB cKO) mice, as previously described (*8, 43*). All experimental mice were obtained from timed matings of $HEB^{fl/fl}$ x $HEB^{fl/fl;Vav\text{-}iCre}$ mice, giving rise to WT and HEB cKO littermates for experimental use. *Id3* deficient mice (Id3-KO) lacked *Id3* in all cells due to a knock-in/knock-out allele in which the Id3 coding sequence was

replaced with red fluorescent proteins (RFP) (JAX strain # 010983, B6;129S-*Id3*^{tm1Pzg}/J). RFP was not detectable in our analyses due to quenching during intracellular staining. Id3-KO mice were acquired on the E29/B6 background and bred onto the C57Bl/6 background for 8 generations. Id3$^{+/-}$ mice were timed mated together to produce WT and Id3-KO littermates. Mice were bred and maintained in the Comparative Research Facility of the Sunnybrook Research Institute (Toronto, Ontario, Canada) under specific pathogen-free conditions. All animal procedures were approved by the Sunnybrook Research Institute Animal Care Committee.

Timed Matings and Embryo Harvest

Timed matings were performed by setting up mating pairs (day 0) and separating them ~16 hrs later. Embryos were harvested after 18 days (E18). Fetal thymuses were dissected, and single cell suspensions were generated by mechanical disruption and filtered through 40-micron mesh. Cells were resuspended in 1X HBSS/BSA for sorting or flow cytometry. Embryos were processed and analyzed separately, and tail tissue was collected for genotyping of fetal mice. Genotyping was performed as previously described (*45*).

Flow cytometry

Antibodies were purchased from eBiosciences (San Diego, California, USA), Biolegend (San Diego, California, USA) and BD Biosciences (Mississauga, Ontario, Canada). For flow cytometry, cells were washed and incubated with Fc blocking antibody (BD Biosciences), followed by extracellular staining for surface CD4 (clone GK1.5), CD8α (clone 53–6.7), CD3 (clone 145-2C11), TCRγδ (clone GL3), Vγ4 (Vγ2; clone UC3-10A6), Vγ5 (Vγ3; clone 536), Vγ1 (Vγ1.1; clone 2.11), CD27 (clone LG3-1A10), CD24 (clone M1/ 69), CD73 (clone TY11.8), and CD25 (clone PC615). To assess functional capacities, cells were stimulated by incubation for four h with PMA (50 ng/ml) and Ionomycin (500 ng/ml) in the presence of Brefeldin A (5mg/ml;

eBioscience), washed with 1X HBSS/BSA, and incubated with Fc block before staining for surface epitopes. Cells were then fixed and permeabilized (Fix and Perm Cell Permeabilization Kit; eBioscience) and stained with antibodies against IL-17A (clone eBio17B7). For intracellular transcription factor staining, the cells were fixed, permeabilized (FoxP3 Staining Kit, eBioscience) and stained for MAF (clone sym0F1), and PLZF (clone R17-809). All flow cytometric analyses were performed using Becton-Dickenson (BD) LSRII, Fortessa, or SymphonyA5-SE cytometers. FACSDiva and FlowJo software were used for analysis. Sorting was performed on BD ARIA and BD Fusion sorters.

Cell culture

SCID.adh cells, which have been engineered to expresses a surface human IL-2Ra (TAC):CD3epsilon chimeric signaling molecule on the surface, were cultured as previously described (*84*). Cells were transduced with MIGR1 encoding GFP only, or MIGR1 encoding GFP and HEBAlt. GFP^+ cells were sorted, expanded, and cultured overnight on plates coated with anti-TAC antibody at 5ug/mL in 500 ul of PBS, or PBS only as control. Cells were analyzed by flow cytometry for expression of CD25, and for mRNA expression of *Id3* by qRT-PCR.

RNA extraction and qRT-PCR

Total RNA was extracted from cells using TRIzol® Reagent (Invitrogen) and reverse-transcribed into complementary DNA using Superscript III (Invitrogen). Reactions for qRT-PCR were prepared using PowerUp SYBR™ Green Master Mix (ThermoFisher) or Luna® Universal qPCR Master Mix (NEB) and 0.5 μM of primers. The qRT-PCR reaction was run and analyzed using an Applied Biosystems 7500 Fast Real-Time PCR System (ThermoFisher) and a QuantStudio™ 5 Real-Time PCR System (ThermoFisher). Values from the qRT-PCR reactions were normalized to *β-actin* values, and relative expression values were calculated by the delta Ct method.

Single-cell RNA sequencing (scRNA-seq) of WT and HEB cKO γδ T cells

E18 fetal thymuses from HEB cKO mice were dissected from embryos and individually pressed through a 40-micron mesh with a syringe plunger to create single cell suspensions. Cells were incubated with Fc block for 30 min on ice. Small aliquots from each sample were stained with CD4, CD8, and CD3 to assess genotypes, with a lack of DP indicating HEB deletion, and genotypes were verified by PCR. Five WT and five HEB cKO littermates were pooled by genotype, stained, and sorted for TCRγδ^{+}CD3^{+} cells. Samples were not hash-tagged as this technology was not available at the time of the experiments. Single cells were isolated using the 10X Chromium controller and barcoded libraries were generated using the Chromium Next GEM Single Cell 5' Kit v2 (Dual Index) (10X Genomics) at the Princess Margaret Genomics Facility (Toronto, ON, Canada). Next generation Illumina sequencing was performed to a depth of ~20,000 reads.

scRNA-seq of WT and Id3-KO DN fetal thymocytes

E18 fetal thymuses from Id3-KO mice were dissected from embryos, pressed through mesh as above, and incubated with Fc block. Embryos were genotyped by PCR, and thymocytes were pooled according to genotype (3 WT and 3 Id3-KO mice). DN cells were enriched by magnetic sorting using anti-CD4 and anti-CD8 microbeads according to manufacturer's instructions (Miltenyi Biotech). Flow-through (CD4^{-}CD8^{-}) cells were processed in-house using the Chromium Next GEM Single Cell 3' Kit v2 (Dual Index) (10X Genomics).

scRNA-seq data analysis of WT and HEB cKO γδ T cells

FASTQ raw data files were aligned to the mm10 genome using Cell Ranger version 1.1.7 (10X Genomics) (*85*). Matrix files were analyzed using programs in R Seurat version 4.4 (*46*), as

detailed in the R-Markdown files. WT and HEB cKO datasets were processed for quality control by excluding cells with more than 7% mitochondrial genes, less than 1000 unique genes, and/or less than 4000 transcripts, resulting in 1272 WT cells and 1951 HEB cKO cells for further analysis. Filtered WT and HEB cKO datasets were merged, and SCTransform was applied to the merged dataset. Cell cycle regression was performed to mitigate the influence of cell cycle heterogeneity on clustering, and cells expressing high levels of *Lyz2* were excluded to remove most myeloid cells. PCA analysis was performed (RunPCA) and used to compute a nearest neighbor graph (FindNeighbors) and identify clusters (FindClusters). UMAP plots were generated using RunUMAP and displayed using DimPlot_scCustom. FindMarkers was used to identify the top ten most differentially expressed genes between clusters which were visualized by heatmap (DoHeatmap).

Generation of gene lists and module scores

To construct an unbiased and comprehensive list of genes diagnostic for different stages and lineages of γδ T cell development, we collected lists of differentially expressed genes from eight publications characterizing γδ T cell subsets in the fetal thymus, adult thymus, and adult peripheral tissues (*13, 21, 47-51, 86*). Genes were filtered to remove those involved in cell cycle and metabolism, as well as NK cell receptor genes. Lists were combined, duplicates were removed, and a final list of 87 genes was obtained (Suppl. Table 1). This list was used for computation of the top ten genes per cluster that were most differentially expressed from all other clusters, visualized as a Clustered DotPlot. Comparisons with the source literature and the Immunological Genome Project (*87*) were used to categorize the clusters. γδTe1 and γδTe2 represent two types of early γδ T cell subsets with random assignments into “1” and “2”.

As developmental stages are continuous, not discrete, some genes were present in more than one module; however, scores were based on all genes in each module. Genes in each module are listed below.

gdTe1: *Ccr9, Sox13, Cpa3, Etv5, Sox5, Tox2, Ccr2, Igfbp4, Blk, Lmo4, Slamf1, Ifngr1, Rorc, Maf, Icos*

gdTe2: *Hivep3, Cd28, Themis, Slamf6, Sell, Igfbp4, Cd24a, Gzma*

gdT17p: *Blk, Il17re, Vdr, Il17a, Lmo4, Slamf1, Ifngr1, Rorc, Maf, Icos*

gdT17: *Il18r1, Il7r, Id2, Il23r, Il1r1, Cd44*

gdT1p: *Klf2, Nrgn, Cd2, Ms4a4b, Prkch, Nr4a1, Id3*

gdT1: *S1pr1, Eomes, Slamf7, Tyrobp, Ifitm1, Fcer1g, Tbx21, Gzmb*

abT: *Cd8a, Notch1, Cd8b1, Rag1, Rag2, Rmnd5a*

Module location and intensity in WT versus HEB cKO cells were visualized using split UMAPs. Comparisons of the expression of single genes between WT and HEB cKO clusters were shown using split violin plots. To compare Clusters 1 and 4, we performed FindMarkers using the Wilcox test, with a minimum of three cells per feature and three cells per group. Differentially expressed genes were displayed using an Enhanced Volcano Plot, with significance set at $\log_2$Fold change > 0.5 and $-\log_{10}P < 10^{26}$.

scRNA-seq data analysis of WT and Id3-KO DN thymocytes

The following analyses were conducted on the Id3-KO dataset. FASTQ raw data files were aligned to the mm39 genome using Cell Ranger. R-Seurat programs were used to filter the cells as described above in the HEB cKO dataset, resulting in 2323 WT cells and 2893 Id3-KO cells for further analysis. Datasets were merged and subjected to SCTransform as above. PCA plots were generated and used to construct UMAP plots depicting clusters in merged datasets and distribution of WT versus Id3-KO cells within each cluster by UMAP (see R-markdown file). Feature plots and violin plots were used to identify clusters with γδ T cell characteristics, which were subsetted using FindClusters. ClusteredDotPlot was used to visualize the top eight most differentially expressed genes within the curated gene set described above. Split violin plots were generated to show relative expression of early and late γδ T cell genes in WT versus HEB cKO cells within each cluster.

Gene ontology analysis

Genes differentially expressed between Cluster 1 and Cluster 4 with a significance of $Log_2Fc > 0.25$ and adjusted P value < 0.001 (Suppl. Table 2) were submitted to ShinyGO 8.0 (*88*) for gene ontogeny analysis. Pathway inclusion was set at a minimum of 5 genes with a false discovery rate (FDR) of 0.05. Genes were analyzed using the Kyoto Encyclopedia of Genes and Genomics (KEGG) pathway database (*89*) (Suppl. Table 3). Results were visualized as a bar graph showing Fold Enrichment (numbers) and -log10(FDR) values (colors).

Alignment of ChIP-seq data

ChIP-seq data for Rag DN3 cells bound to HEB (Rag DN3-HEB) or E2A (Rag DN3-E2A) were generated as previously described (*63*). All other files were obtained from the Cistrome database (*90*) and aligned to the mouse genome (mm38) using the Integrated Genomics Viewer (*91*). Sources were as follows: Thy anti-TCRb-Egr2, GEO accession # GSM845900 (*64*); Rag d7

aCD3-RNA pol II, GEO accession # GSM1340642 (*65*); DN3 H3K27me3, GEO accession # GSM1498423, and DN4 H3K27me3, GEO accession # GSM1498422 (*92*).

REFERENCES

1. J. C. Ribot, N. Lopes, B. Silva-Santos, γδ T cells in tissue physiology and surveillance. *Nature Reviews Immunology* **21**, 221-232 (2021).
2. A. C. Kohlgruber *et al.*, gammadelta T cells producing interleukin-17A regulate adipose regulatory T cell homeostasis and thermogenesis. *Nat Immunol* **19**, 464-474 (2018).
3. P. H. Papotto, A. Reinhardt, I. Prinz, B. Silva-Santos, Innately versatile: gammadelta17 T cells in inflammatory and autoimmune diseases. *J Autoimmun* **87**, 26-37 (2018).
4. K. Alves de Lima *et al.*, Meningeal gammadelta T cells regulate anxiety-like behavior via IL-17a signaling in neurons. *Nat Immunol* **21**, 1421-1429 (2020).
5. W. Haas, P. Pereira, S. Tonegawa, Gamma/delta cells. *Annu Rev Immunol* **11**, 637-685 (1993).
6. K. Shibata *et al.*, Identification of CD25+ gamma delta T cells as fetal thymus-derived naturally occurring IL-17 producers. *J Immunol* **181**, 5940-5947 (2008).
7. I. Sandrock *et al.*, Genetic models reveal origin, persistence and non-redundant functions of IL-17-producing gammadelta T cells. *J Exp Med* **215**, 3006-3018 (2018).
8. T. S. H. In *et al.*, HEB is required for the specification of fetal IL-17-producing gammadelta T cells. *Nat Commun* **8**, 2004 (2017).
9. W. L. Havran, J. P. Allison, Origin of Thy-1+ dendritic epidermal cells of adult mice from fetal thymic precursors. *Nature* **344**, 68-70 (1990).
10. G. Turchinovich, A. C. Hayday, Skint-1 identifies a common molecular mechanism for the development of interferon-gamma-secreting versus interleukin-17-secreting gammadelta T cells. *Immunity* **35**, 59-68 (2011).
11. T. B. Buus, N. Odum, C. Geisler, J. P. H. Lauritsen, Three distinct developmental pathways for adaptive and two IFN-gamma-producing gammadelta T subsets in adult thymus. *Nat Commun* **8**, 1911 (2017).
12. E. L. Y. Chen *et al.*, Ontogenic timing, T cell receptor signal strength, and Notch signaling direct γδ T cell functional differentiation in vivo. *Cell Rep* **35**, 109227 (2021).
13. T. Yang *et al.*, RORgammat(+) c-Maf(+) Vgamma4(+) gammadelta T cells are generated in the adult thymus but do not reach the periphery. *Cell Rep* **42**, 113230 (2023).
14. N. Schmolka *et al.*, Epigenetic and transcriptional signatures of stable versus plastic differentiation of proinflammatory gammadelta T cell subsets. *Nat Immunol* **14**, 1093-1100 (2013).
15. K. Grigoriadou, L. Boucontet, P. Pereira, Most IL-4-producing gamma delta thymocytes of adult mice originate from fetal precursors. *J Immunol* **171**, 2413-2420 (2003).
16. M. Ciofani, J. C. Zuniga-Pflucker, Determining gammadelta versus alphass T cell development. *Nat Rev Immunol* **10**, 657-663 (2010).
17. E. C. Dudley, M. Girardi, M. J. Owen, A. C. Hayday, Alpha beta and gamma delta T cells can share a late common precursor. *Curr Biol* **5**, 659-669 (1995).
18. A. Dutta, B. Zhao, P. E. Love, New insights into TCR beta-selection. *Trends Immunol* **42**, 735-750 (2021).
19. N. Malhotra *et al.*, A network of high-mobility group box transcription factors programs innate interleukin-17 production. *Immunity* **38**, 681-693 (2013).
20. E. E. Gray *et al.*, Deficiency in IL-17-committed Vgamma4(+) gammadelta T cells in a spontaneous Sox13-mutant CD45.1(+) congenic mouse substrain provides protection from dermatitis. *Nat Immunol* **14**, 584-592 (2013).

21. Sagar *et al.*, Deciphering the regulatory landscape of fetal and adult γδ T-cell development at single-cell resolution. *Embo j* **39**, e104159 (2020).
22. M. K. Zuberbuehler *et al.*, The transcription factor c-Maf is essential for the commitment of IL-17-producing gammadelta T cells. *Nat Immunol* **20**, 73-85 (2019).
23. P. Zarin, G. W. Wong, M. Mohtashami, D. L. Wiest, J. C. Zuniga-Pflucker, Enforcement of gammadelta-lineage commitment by the pre-T-cell receptor in precursors with weak gammadelta-TCR signals. *Proc Natl Acad Sci U S A* **111**, 5658-5663 (2014).
24. S. Y. Lee, J. Stadanlick, D. J. Kappes, D. L. Wiest, Towards a molecular understanding of the differential signals regulating alphabeta/gammadelta T lineage choice. *Semin Immunol* **22**, 237-246 (2010).
25. M. C. Haks *et al.*, Attenuation of gammadeltaTCR signaling efficiently diverts thymocytes to the alphabeta lineage. *Immunity* **22**, 595-606 (2005).
26. P. Zarin, E. L. Chen, T. S. In, M. K. Anderson, J. C. Zuniga-Pflucker, Gamma delta T-cell differentiation and effector function programming, TCR signal strength, when and how much? *Cell Immunol* **296**, 70-75 (2015).
27. S. P. Fahl *et al.*, Role of a selecting ligand in shaping the murine gammadelta-TCR repertoire. *Proc Natl Acad Sci U S A* **115**, 1889-1894 (2018).
28. R. Muro *et al.*, gammadeltaTCR recruits the Syk/PI3K axis to drive proinflammatory differentiation program. *J Clin Invest* **128**, 415-426 (2018).
29. P. Zarin *et al.*, Integration of T-cell receptor, Notch and cytokine signals programs mouse gammadelta T-cell effector differentiation. *Immunol Cell Biol* **96**, 994-1007 (2018).
30. M. L. Michel *et al.*, Interleukin 7 (IL-7) selectively promotes mouse and human IL-17-producing gammadelta cells. *Proc Natl Acad Sci U S A* **109**, 17549-17554 (2012).
31. G. Bain *et al.*, Regulation of the helix-loop-helix proteins, E2A and Id3, by the Ras-ERK MAPK cascade. *Nat Immunol* **2**, 165-171 (2001).
32. S. P. Fahl, D. J. Kappes, D. L. Wiest, in *Signaling Mechanisms Regulating T Cell Diversity and Function,* J. Soboloff, D. J. Kappes, Eds. (Boca Raton (FL), 2018), pp. 85-104.
33. S. Y. Lee *et al.*, Noncanonical mode of ERK action controls alternative alphabeta and gammadelta T cell lineage fates. *Immunity* **41**, 934-946 (2014).
34. M. Munoz-Ruiz *et al.*, TCR signal strength controls thymic differentiation of discrete proinflammatory gammadelta T cell subsets. *Nat Immunol* **17**, 721-727 (2016).
35. M. E. Jones, Y. Zhuang, Stage-specific functions of E-proteins at the beta-selection and T-cell receptor checkpoints during thymocyte development. *Immunol Res* **49**, 202-215 (2011).
36. L. M. D'Cruz, K. C. Lind, B. B. Wu, J. K. Fujimoto, A. W. Goldrath, Loss of E protein transcription factors E2A and HEB delays memory-precursor formation during the CD8+ T-cell immune response. *Eur J Immunol* **42**, 2031-2041 (2012).
37. M. E. Jones-Mason *et al.*, E protein transcription factors are required for the development of CD4(+) lineage T cells. *Immunity* **36**, 348-361 (2012).
38. J. P. Leung *et al.*, HEB Restrains Effector Gene Expression during Early CD8(+) Memory Precursor T Cell Differentiation. *Mol Cell Biol*, 1-18 (2025).
39. J. P. Lauritsen *et al.*, Marked induction of the helix-loop-helix protein Id3 promotes the gammadelta T cell fate and renders their functional maturation Notch independent. *Immunity* **31**, 565-575 (2009).

40. J. S. Heilig, S. Tonegawa, Diversity of murine gamma genes and expression in fetal and adult T lymphocytes. *Nature* **322**, 836-840 (1986).
41. M. P. Lefranc, IMGT, the international ImMunoGeneTics database. *Nucleic Acids Res* **31**, 307-310 (2003).
42. R. M. Baldarelli *et al.*, Mouse Genome Informatics: an integrated knowledgebase system for the laboratory mouse. *Genetics* **227**, (2024).
43. E. Welinder *et al.*, The transcription factors E2A and HEB act in concert to induce the expression of FOXO1 in the common lymphoid progenitor. *Proc Natl Acad Sci U S A* **108**, 17402-17407 (2011).
44. R. Barndt, M. F. Dai, Y. Zhuang, A novel role for HEB downstream or parallel to the pre-TCR signaling pathway during alpha beta thymopoiesis. *J Immunol* **163**, 3331-3343 (1999).
45. J. Wojciechowski, A. Lai, M. Kondo, Y. Zhuang, E2A and HEB are required to block thymocyte proliferation prior to pre-TCR expression. *J Immunol* **178**, 5717-5726 (2007).
46. Y. Hao *et al.*, Integrated analysis of multimodal single-cell data. *Cell* **184**, 3573-3587 e3529 (2021).
47. S. K. Mistri *et al.*, SLAM/SAP signaling regulates discrete gammadelta T cell developmental checkpoints and shapes the innate-like gammadelta TCR repertoire. *Elife* **13**, (2024).
48. N. A. Spidale *et al.*, Interleukin-17-Producing gammadelta T Cells Originate from SOX13(+) Progenitors that Are Independent of gammadeltaTCR Signaling. *Immunity* **49**, 857-872 e855 (2018).
49. Y. Liu *et al.*, Single-Cell Profiling Reveals Divergent, Globally Patterned Immune Responses in Murine Skin Inflammation. *iScience* **23**, 101582 (2020).
50. K. Narayan *et al.*, Intrathymic programming of effector fates in three molecularly distinct gammadelta T cell subtypes. *Nat Immunol* **13**, 511-518 (2012).
51. D. Inacio *et al.*, Signature cytokine-associated transcriptome analysis of effector gammadelta T cells identifies subset-specific regulators of peripheral activation. *Nat Immunol*, (2025).
52. C. Murre, Helix-loop-helix proteins and the advent of cellular diversity: 30 years of discovery. *Genes Dev* **33**, 6-25 (2019).
53. F. Coffey *et al.*, The TCR ligand-inducible expression of CD73 marks gammadelta lineage commitment and a metastable intermediate in effector specification. *J Exp Med* **211**, 329-343 (2014).
54. T. B. Buus, C. Geisler, J. P. Lauritsen, The major diversification of Vgamma1.1(+) and Vgamma2(+) thymocytes in mice occurs after commitment to the gammadelta T-cell lineage. *Eur J Immunol* **46**, 2363-2375 (2016).
55. Y. Lu, X. Cao, X. Zhang, D. Kovalovsky, PLZF Controls the Development of Fetal-Derived IL-17+Vgamma6+ gammadelta T Cells. *J Immunol* **195**, 4273-4281 (2015).
56. T. Kreslavsky *et al.*, TCR-inducible PLZF transcription factor required for innate phenotype of a subset of gammadelta T cells with restricted TCR diversity. *Proc Natl Acad Sci U S A* **106**, 12453-12458 (2009).
57. E. S. Alonzo *et al.*, Development of promyelocytic zinc finger and ThPOK-expressing innate gamma delta T cells is controlled by strength of TCR signaling and Id3. *J Immunol* **184**, 1268-1279 (2010).

58. B. Zhang, Y. Y. Lin, M. Dai, Y. Zhuang, Id3 and Id2 act as a dual safety mechanism in regulating the development and population size of innate-like gammadelta T cells. *J Immunol* **192**, 1055-1063 (2014).
59. J. Barros-Martins *et al.*, Effector gammadelta T Cell Differentiation Relies on Master but Not Auxiliary Th Cell Transcription Factors. *J Immunol* **196**, 3642-3652 (2016).
60. J. A. Hall *et al.*, Transcription factor RORalpha enforces stability of the Th17 cell effector program by binding to a Rorc cis-regulatory element. *Immunity* **55**, 2027-2043 e2029 (2022).
61. B. C. Lo *et al.*, The orphan nuclear receptor ROR alpha and group 3 innate lymphoid cells drive fibrosis in a mouse model of Crohn's disease. *Sci Immunol* **1**, (2016).
62. H. Xi, R. Schwartz, I. Engel, C. Murre, G. J. Kersh, Interplay between RORgammat, Egr3, and E proteins controls proliferation in response to pre-TCR signals. *Immunity* **24**, 813-826 (2006).
63. S. P. Fahl *et al.*, The E protein-TCF1 axis controls gammadelta T cell development and effector fate. *Cell Rep* **34**, 108716 (2021).
64. M. P. Seiler *et al.*, Elevated and sustained expression of the transcription factors Egr1 and Egr2 controls NKT lineage differentiation in response to TCR signaling. *Nat Immunol* **13**, 264-271 (2012).
65. A. Pekowska *et al.*, H3K4 tri-methylation provides an epigenetic signature of active enhancers. *EMBO J* **30**, 4198-4210 (2011).
66. M. Carleton *et al.*, Signals transduced by CD3epsilon, but not by surface pre-TCR complexes, are able to induce maturation of an early thymic lymphoma in vitro. *J Immunol* **163**, 2576-2585 (1999).
67. I. Engel, C. Murre, E2A proteins enforce a proliferation checkpoint in developing thymocytes. *EMBO J* **23**, 202-211 (2004).
68. D. Wang *et al.*, Context-dependent regulation of hematopoietic lineage choice by HEBAlt. *J Immunol* **185**, 4109-4117 (2010).
69. D. Wang *et al.*, The basic helix-loop-helix transcription factor HEBAlt is expressed in pro-T cells and enhances the generation of T cell precursors. *J Immunol* **177**, 109-119 (2006).
70. K. Yoganathan *et al.*, Regulation of the Signal-Dependent E Protein HEBAlt Through a YYY Motif Is Required for Progression Through T Cell Development. *Front Immunol* **13**, 848577 (2022).
71. S. Scaramuzzino *et al.*, Single-cell transcriptomics uncovers an instructive T-cell receptor role in adult gammadelta T-cell lineage commitment. *EMBO J* **41**, e110023 (2022).
72. E. Kashani *et al.*, A clonotypic Vgamma4Jgamma1/Vdelta5Ddelta2Jdelta1 innate gammadelta T-cell population restricted to the CCR6(+)CD27(-) subset. *Nat Commun* **6**, 6477 (2015).
73. G. Bain, W. J. Romanow, K. Albers, W. L. Havran, C. Murre, Positive and negative regulation of V(D)J recombination by the E2A proteins. *J Exp Med* **189**, 289-300 (1999).
74. M. Nozaki *et al.*, Regulation of TCR Vgamma2 gene rearrangement by the helix-loop-helix protein, E2A. *Int Immunol* **23**, 297-305 (2011).
75. B. Hao, M. S. Krangel, Long-distance regulation of fetal V(delta) gene segment TRDV4 by the Tcrd enhancer. *J Immunol* **187**, 2484-2491 (2011).
76. M. Braunstein, M. K. Anderson, HEB-deficient T-cell precursors lose T-cell potential and adopt an alternative pathway of differentiation. *Mol Cell Biol* **31**, 971-982 (2011).

77. M. Miyazaki *et al.*, The E-Id Protein Axis Specifies Adaptive Lymphoid Cell Identity and Suppresses Thymic Innate Lymphoid Cell Development. *Immunity* **46**, 818-834 e814 (2017).
78. P. M. Brauer *et al.*, Modeling altered T-cell development with induced pluripotent stem cells from patients with RAG1-dependent immune deficiencies. *Blood* **128**, 783-793 (2016).
79. M. E. Parker *et al.*, Restriction of innate Tgammadelta17 cell plasticity by an AP-1 regulatory axis. *Nat Immunol* **26**, 1299-1314 (2025).
80. M. K. Anderson, Shifting gears: Id3 enables recruitment of E proteins to new targets during T cell development and differentiation. *Front Immunol* **13**, 956156 (2022).
81. R. Schwartz, I. Engel, M. Fallahi-Sichani, H. T. Petrie, C. Murre, Gene expression patterns define novel roles for E47 in cell cycle progression, cytokine-mediated signaling, and T lineage development. *Proc Natl Acad Sci U S A* **103**, 9976-9981 (2006).
82. J. de Boer *et al.*, Transgenic mice with hematopoietic and lymphoid specific expression of Cre. *Eur J Immunol* **33**, 314-325 (2003).
83. S. Siegemund, J. Shepherd, C. Xiao, K. Sauer, hCD2-iCre and Vav-iCre mediated gene recombination patterns in murine hematopoietic cells. *PLoS One* **10**, e0124661 (2015).
84. M. K. Anderson, A. H. Weiss, G. Hernandez-Hoyos, C. J. Dionne, E. V. Rothenberg, Constitutive expression of PU.1 in fetal hematopoietic progenitors blocks T cell development at the pro-T cell stage. *Immunity* **16**, 285-296 (2002).
85. G. X. Zheng *et al.*, Massively parallel digital transcriptional profiling of single cells. *Nat Commun* **8**, 14049 (2017).
86. A. du Halgouet *et al.*, Multimodal profiling reveals site-specific adaptation and tissue residency hallmarks of gammadelta T cells across organs in mice. *Nat Immunol* **25**, 343-356 (2024).
87. T. S. Heng, M. W. Painter, C. Immunological Genome Project, The Immunological Genome Project: networks of gene expression in immune cells. *Nat Immunol* **9**, 1091-1094 (2008).
88. S. X. Ge, D. Jung, R. Yao, ShinyGO: a graphical gene-set enrichment tool for animals and plants. *Bioinformatics* **36**, 2628-2629 (2020).
89. M. Kanehisa, M. Furumichi, Y. Sato, Y. Matsuura, M. Ishiguro-Watanabe, KEGG: biological systems database as a model of the real world. *Nucleic Acids Res* **53**, D672-D677 (2025).
90. R. Zheng *et al.*, Cistrome Data Browser: expanded datasets and new tools for gene regulatory analysis. *Nucleic Acids Res* **47**, D729-D735 (2019).
91. J. T. Robinson *et al.*, Integrative genomics viewer. *Nat Biotechnol* **29**, 24-26 (2011).
92. A. Oravecz *et al.*, Ikaros mediates gene silencing in T cells through Polycomb repressive complex 2. *Nat Commun* **6**, 8823 (2015).

Data and materials availability. Matrix files and R-markdown code have been deposited to the Dryad repository and can be accessed at:

HEB-WT scRNA-seq matrix files and R-markdown code

https://doi.org/10.5061/dryad.08kprr5cq

HEB cKO scRNA-seq matrix files

https://doi.org/10.5061/dryad.qv9s4mwqh

Id3-WT scRNA-seq matrix files and R-markdown code

https://doi.org/10.5061/dryad.j6q573nqd

Id3-KO scRNA-seq matrix files

https://doi.org/10.5061/dryad.x0k6djhvj

Acknowledgments. We would like to thank Lisa Wells, Madeline Harvey, Vivien Musiime, and the SRI Animal Facility for excellent mouse care. We thank Lily Rast for assistance with cell culture, and Yuan Zhuang for provision of the HEB cKO mice. We are indebted to the SickKids Flow Cytometry Core (supported by the Canadian Foundation for Innovation (CFI) and the SickKids' Foundation) for antibody panel design and high parameter flow cytometry analysis, and the SRI Flow Cytometry and Microscopy Core for flow cytometry and sorting. We also thank the UHN Princess Margaret Genomics Facility for construction of the WT and HEB cKO scRNA-seq libraries. The Digital Research Alliance of Canada (RRG #5070) provided cloud computing capacity for scRNA-seq data analysis.

Funding. This work was supported by the Canadian Institutes for Health Research (CIHR; PJT 153058 to MKA, FDN154332 and PJT192050 to JCZP, and PJT165973 to CJG), National Institutes of Health (NIH: 1P01AI102853-06) to MKA, JCZP, DLW and CM, and a CFI John Evans Fund Leaders' Infrastructure Grant to CJG (#37562). JS was supported by an American Association for Immunologists Careers in Immunology Award and a CIHR Postdoctoral Fellowship. VR was supported by a CIHR Postdoctoral Fellowship, and HW was the recipient of an Ontario Graduate Scholarship.

Author contributions. J.S.S. and M.K.A. conceptualized the study. E.S.R., M.S.G, and C.J.G. developed high parameter flow cytometry panels. J.S.S., E.S.R., and J.D.R. collected the flow cytometry data, and J.S.S. sorted cells for the scRNA-seq experiments. M.K.A. analyzed the scRNA-seq data, assisted by H.W. and V.R., and generated the figures. V.R. and H.W. performed the *Id3* scRNA-seq experiment. J.D.R. and J.J.L. performed the cell culture experiments. Funding

was acquired by M.K.A., J.C.Z.P, D.L.W. and C.M. M.K.A., J.C.Z.P., D.L.W, and C.M. interpreted the data and formed the model. M.K.A. wrote the first draft of the manuscript, and all authors contributed to the final manuscript.

Conflict of Interest

The authors declare there are no conflicts of interest.

FIGURE LEGENDS

Figure 1. Partial block in early γδ T cell development and decrease in Vγ4 cells in HEB-deficient mice. A. Stages of fetal mouse γδ T cell development. Thymocytes at the DN2 ($CD4^-CD8^-CD44^+CD25^+$) and DN3 ($CD4^-CD8^-CD44^-CD25^+$) stages of T cell development rearrange and express TCRγ, TCRδ, and TCRβ genes. DN3 cells with productive TCRβ chains expressing a pre-TCR are directed into the αβ-T cell lineage, characterized by upregulation of CD4 and CD8. Cells that receive a γδTCR signal are directed into the γδ T cell lineage (γδTe, early γδ T cells). Surface expression of γδTCR precedes γδTCR signaling; thus, not all $\gamma\delta TCR^+$ cells have committed to the γδ T cell lineage, and failure to be triggered by a γδTCR ligand can divert them into the αβ T cell lineage (dotted line). $\gamma\delta TCR^+$ cells receiving a strong signal become $CD73^+$ γδT1 cell progenitors (γδT1p) that mature into IFNγ producing γδT1 cells, whereas cells that receive an intermediate signal become γδT17 cell progenitors (γδT17p) that mature into IL-17 producing γδT17 cells. Downregulation of CD24 and CD27, and upregulation of CD44, marks maturation of γδT17 cells, whereas γδT1 cell maturation is characterized by downregulation of CD24 and maintenance of CD73 and CD27 expression. B. γδ T cell nomenclature. Vγ and Vδ chain genes and proteins can be identified by several different naming systems. Here we use the Tonegawa nomenclature to refer to the proteins, and the International Immunogenetics Information System (IMGT) for the genes and transcripts. R-Seurat generated plots use the Mouse Genome Informatics (MGI) nomenclature. The numbering for genes and proteins in these three systems are identical except for the TRDV4 gene, which encodes the Vγ1 protein (highlighted in red). C. Absolute numbers of cells per thymus in WT (blue) and HEB cKO (orange) E18 fetal mice. D, E. Percentages of γδ T cells in WT and HEB cKO fetal thymus. F. Absolute number of

γδ T cells per thymus in WT and HEB cKO fetal thymus. G. Flow cytometry plots of Vγ4$^+$ and Vγ1$^+$ cells within the γδ T cell population in WT and HEB cKO fetal thymus. H. Flow cytometry plot of Vγ5 and Vγ6 (Vγ1$^-$Vγ5$^-$) expression on cells within the Vγ1$^-$Vγ4$^-$ population. I. Percentages of Vγ1$^+$, Vγ4$^+$, Vγ5$^+$, and Vγ6$^+$ cells out of all γδ T cells in the WT and HEB cKO fetal thymus. J. Absolute numbers of Vγ1$^+$, Vγ4$^+$, Vγ5$^+$, and Vγ6$^+$ cells per WT and HEB cKO fetal thymus. K. Percentages of immature (CD24$^+$) and mature (CD24$^-$) γδ T cells out of all γδ T cells in each Vγ subset in WT and HEB cKO fetal thymus. L. Expression of IL-17A protein in γδ T cells from E18 thymus stimulated with PMA/ionomycin as assessed by intracellular staining. Blue = WT, orange = HEB cKO. * $p < 0.05$, ** $p < 0.01$, *** $p < 0.001$, *** $p <0.0001$.

Figure 2. Identification of γδ T cell subsets in WT and HEB cKO fetal thymus by scRNA-seq. γδ T cells were sorted from E18 fetal thymuses from WT and HEB cKO mice, pooled according to genotype, and subjected to scRNA-sequencing and analysis. A. UMAP plots depicting merged WT and HEB cKO cells in 8 clusters (0-7). B. Grouped UMAP showing the distribution of WT (blue) and HEB cKO (orange) cells across all clusters. C. Split UMAP plots showing the distribution of cells in WT (left) and HEB cKO (right) clusters; note that cluster 4 is restricted to WT cells, and cluster 1 is heavily biased towards HEB cKO cells. D. Genes previously identified as signatures for developmental and functional γδ T cell subsets were compiled from previously published reports. The top ten most differentially expressed genes from this list were visualized as a clustered dot plot which was used to assign cluster identities. Two clusters corresponding to early γδ T cells (γδTe) were randomly named γδTe1 and γδTe2. E. Numbers of WT (blue) and HEB cKO (orange) cells per cluster. F. Unbiased clustered dot plot of the top ten most differentially expressed genes across all clusters. In the clustered dot plots, the percentage of

cells expressing the gene in each cluster is depicted by the size of the dot, and the color indicates the relative magnitude of expression across clusters.

Figure 3. The αβ T gene program is inflated and the γδT17 precursor gene program is lost in HEB cKO cells. γδ T cells were sorted from E18 fetal thymuses from WT and HEB cKO mice were pooled according to genotype and subjected to scRNA-sequencing and analysis. A, B. Gene modules were generated from subset-biased genes (Fig. 2), and cells were scored for each module. Module scores are depicted as split feature plots, with WT plots on the left and HEB cKO plots on the right. Module scores that characterize γδ T cell subsets are shown in (A), and a module score for the αβ-T lineage is shown in (B). C-G. Split violin plots of genes that typify different γδ T cell subsets as follows: C) γδTe/γδT17p cells, (D) αβ T cells, (E) γδT17 cells, (F) γδT1p/γδT1 cells, and (G) γδT1 cells. Blue = WT, orange = HEB cKO.

Figure 4. Decreases in T cell effector differentiation and TCR signaling genes in γδT17p cells from HEB cKO mice. A. Volcano plots showing differential gene expression in γδT17p cells from WT versus HEB cKO fetal thymus. Genes expressed at higher levels in HEB cKO cells are on the left, and genes expressed at lower levels in HEB cKO cells are on the right. Significance (pink) was set at $Log_2Fc > 0.5$ and $Log_{10}P < 10^{25}$. B. Gene ontology analysis of genes significantly reduced in HEB cKO γδT17p cells relative to WT, with significance set at avg $Log_2Fc > 0.25$ and adjusted P value < 0.001. Bar plots show pathway enrichment (Fold enrichment) and significance by false discovery rate (FDR) for each functional category defined in the KEGG pathway list. Minimum genes for pathway inclusion was set at 5 and FDR cutoff was set at 0.05. C. Relative expression of genes associated with strong TCR signaling in WT and HEB cKO cells in each

cluster. D. Relative expression of *Id3* in immature γδ T cell subsets from WT and HEB cKO mice. E. Split feature plots showing expression of *Id3* across all clusters in WT versus HEB cKO cells. F. Relative expression of *Maf* and *Rorc* in WT versus HEB cKO γδT cell subsets. WT = blue, HEB cKO = orange.

Figure 5. Fetal γδ T cells from Id3-KO mice are defective in CD73 upregulation and IL-17 production. A. Absolute numbers of cells per E18 fetal thymus from WT and Id3-KO littermate mice. B, C. Quantification (B) and flow cytometry plots (C) of the percentages of γδ T cells out of all thymocytes. D, E. Flow cytometry plots (D) and quantification (E) of $V\gamma1^+$ and $V\gamma4^+$ out of all γδ T cells. F. Percentages of $V\gamma5^+$ and $V\gamma6^+$ out of all γδ T cells. G. Flow cytometry plots of CD24 and CD73 expression in $\gamma\delta TCR^+$ cells. H. Quantification of mature ($CD24^-$) $CD73^+$ and $CD73^-$ γδ T cells out of all γδ T cells. I. Flow cytometry plots of expression of CD27 and CD73 expression in unstimulated (top) and stimulated (bottom) γδ T cells. J. Percentages of $CD27^+CD73^+$ cells out of all γδ T cells under unstimulated or stimulated conditions. K, L. Flow cytometry (K) and quantification (L) of the percentages of $CD27^-CD73^-CD24^-$ (primarily mature Vγ6) cells expressing IL-17 in response to stimulation. Blue = WT, pink = Id3-KO. P/I = phorbol 12-myristate 13-acetate (PMA) + ionomycin. * $p < 0.05$, ** $p < 0.01$, *** $p < 0.001$, *** $p < 0.0001$.

Figure 6. Intact γδ T commitment gene program and impaired γδT17 maturation program in Id3-KO mice. A. Flow cytometry plots showing the percentages of cells expressing PLZF and/or MAF in immature ($CD24^+$) Vγ4 and Vγ6 cells, and in mature ($CD24^-$) Vγ6 cells (note that mature Vγ4 cells are not present in the E18 fetal thymus). B. Quantification of the percentages of cells expressing PLZF and MAF (top), PLZF only (middle) or neither (bottom) within the

immature Vγ4 and Vγ6 subsets, and the mature Vγ6 subset. C. Mean fluorescent intensities of PLZF in the $PLZF^{+}MAF^{+}$ and $PLZF^{+}MAF^{-}$ populations within the immature and mature Vγ subsets. D, E. sRNA-seq UMAP plots of γδ T cells as merged (D) or split (E) into WT versus Id3-KO populations. F. Number of WT and Id3-KO cells per cluster. G. Clustered dot plot of curated gene sets used to assign γδT17p, γδTe, γδT17, and γδT1 identities. H. Expression of γδ T cell commitment genes in WT versus Id3-KO cells by cluster. I. Expression of γδT17 maturation genes in WT versus Id3-KO cells by cluster. Blue = WT, pink = Id3-KO. ** $p < 0.01$, *** $p < 0.001$, *** $p < 0.0001$

Figure 7. Synergistic upregulation of *Id3* by HEB and CD3 signaling. A. ChIP-seq data analysis of the binding of HEB, E2A, RNA polymerase, and Egr2, and the extent of H3K27me3 chromatin modification, in DN3 and/or DN4 cells at the *Id3* gene locus, obtained from publicly available datasets (see Materials and Methods for accession numbers). The cell type and antibody used in each experiment are indicated to the right of the tracks. Peaks bound by HEB, E2A, and/or Egr2 are indicated in boxes. Inset shows the *Id3* exons and the adjacent *Gm42329* long non-coding RNA. B. Diagram of experimental design. SCID.adh cells transduced with HEBAlt or control retroviral vectors were cultured for 16 hours in the presence or absence of the anti-TAC antibody, which induces signaling through the CD3 complex. C, E. Flow cytometry plots (C) and quantification (E) of CD25 upregulation with and without stimulation and/or HEB expression. D. *Id3* mRNA expression relative to β-actin as determined by quantitative RT-PCR. Rag = *Rag2*$^{-/-}$ mouse thymocytes, which are arrested at the DN3 stage of development. ** $p < 0.01$, *** $p < 0.001$, *** $p < 0.0001$

Figure 1

A

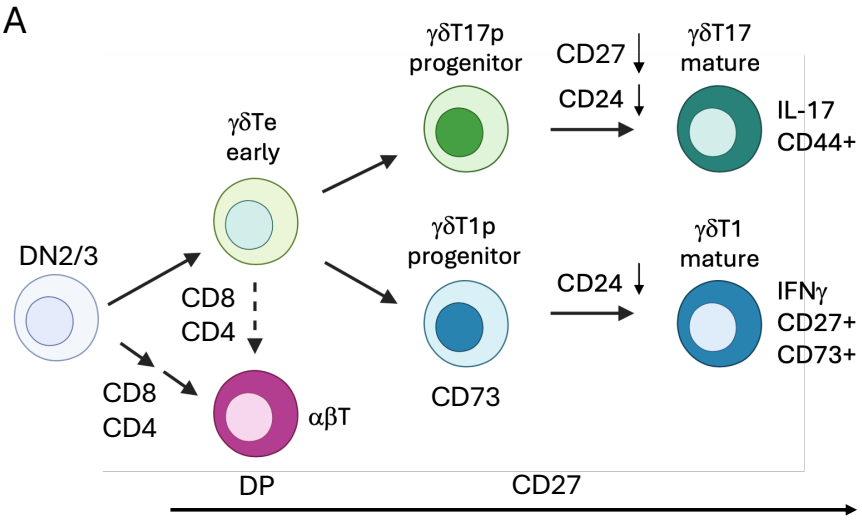

B

Protein	Gene	Gene
Tonegawa	IMGT	MGI
Vγ4	TRGV4	Tcrg-V4
Vγ5	TRGV5	Tcrg-V5
Vγ1	TRGV1	Tcrg-V1
Vγ6	TRGV6	Tcrg-V6
Vδ1	TRDV4	Trdv4
Vδ5	TRDV5	Trdv5

C

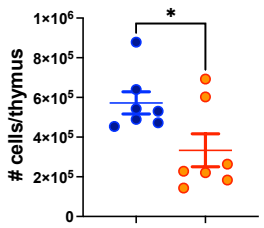

D

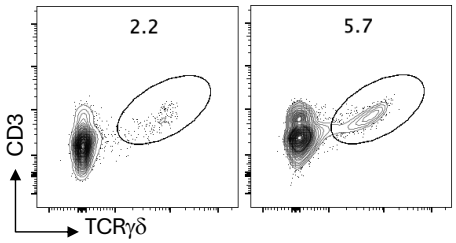

E

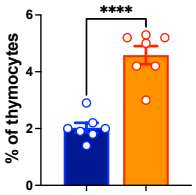

F

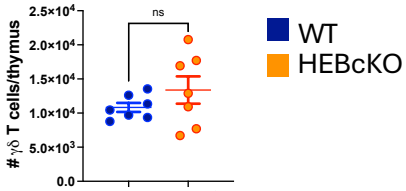

G

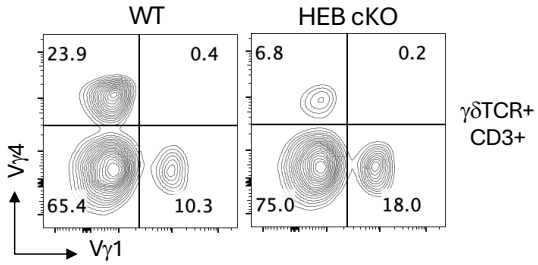

H

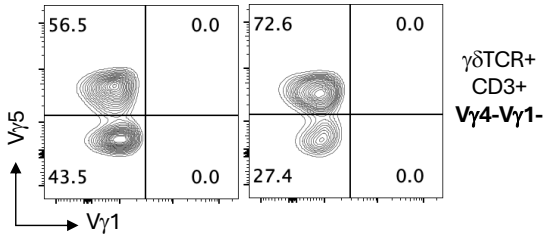

I

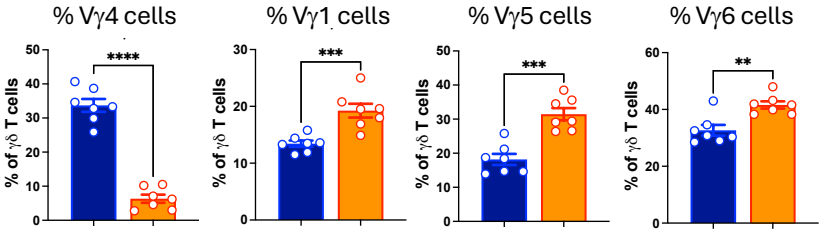

J

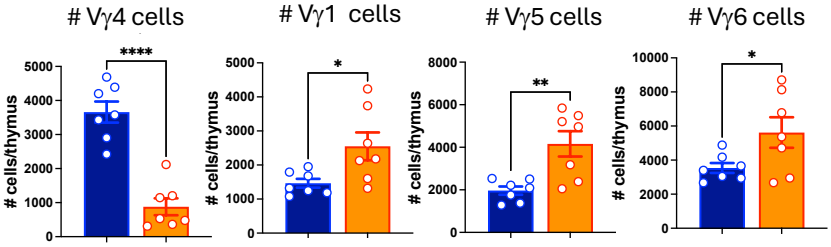

K

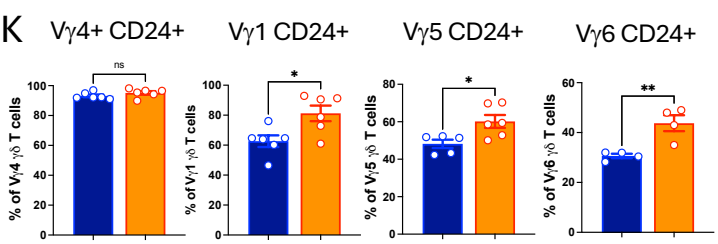

L

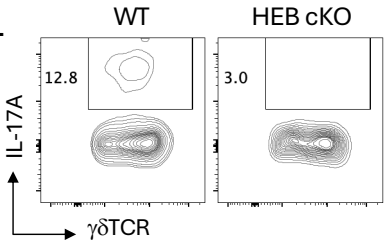

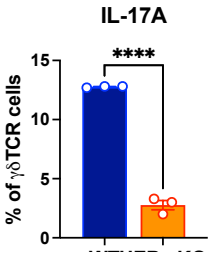

Figure 2

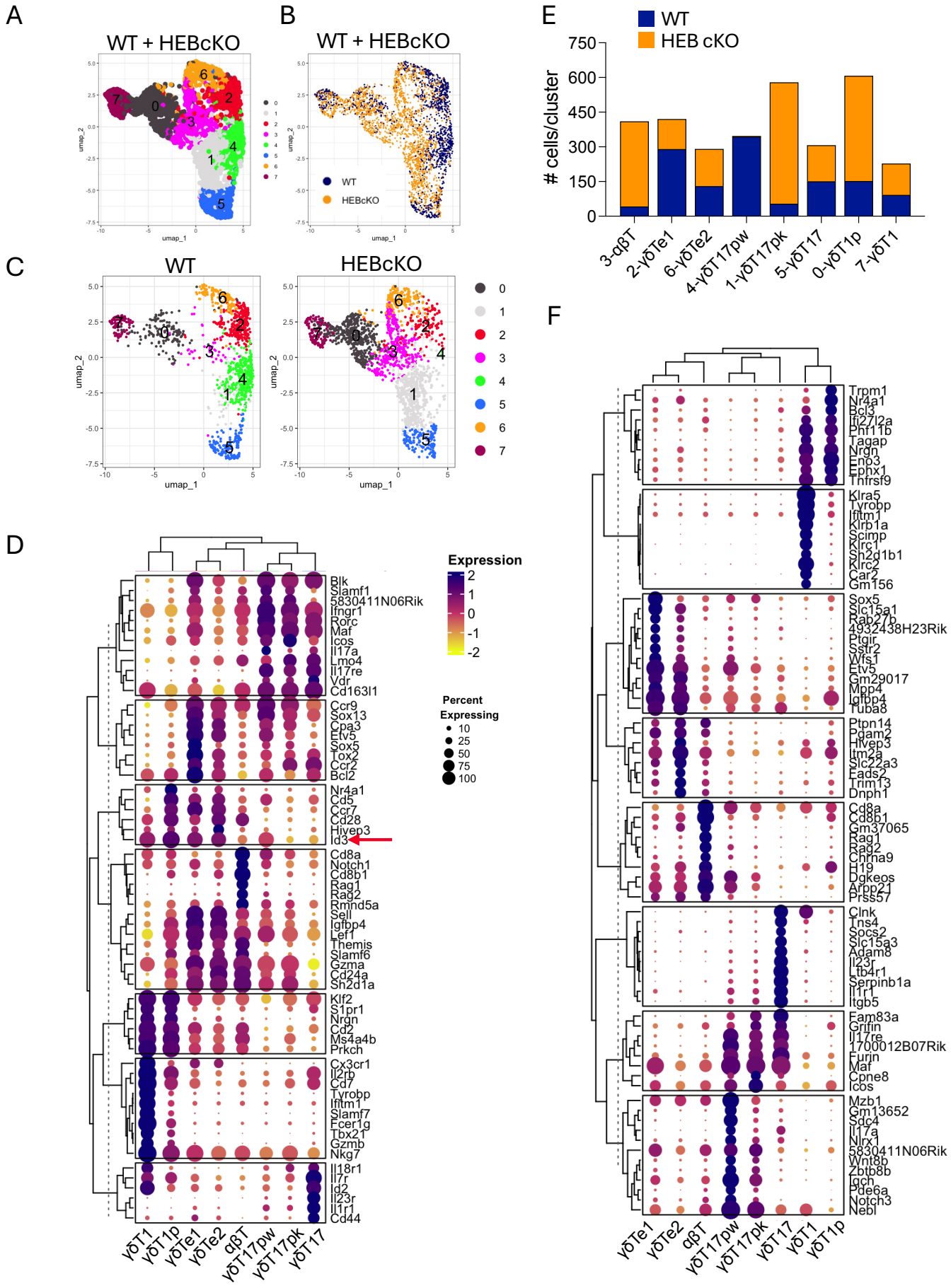
A
WT + HEBcKO
umap_1
umap_2
B
WT + HEBcKO
WT
HEBcKO
C
WT
HEBcKO
0
1
2
3
4
5
6
7
D
Expression
2
1
0
-1
-2
Percent Expressing
10
25
50
75
100
Blk
Slamf1
5830411N06Rik
Ifngr1
Rorc
Maf
Icos
Il17a
Lmo4
Il17re
Vdr
Cd163l1
Ccr9
Sox13
Cpa3
Etv5
Sox5
Tox2
Ccr2
Bcl2
Nr4a1
Cd5
Ccr7
Cd28
Hivep3
Id3
Cd8a
Notch1
Cd8b1
Rag1
Rag2
Rmnd5a
Sell
Igfbp4
Lef1
Themis
Slamf6
Gzma
Cd24a
Sh2d1a
Klf2
S1pr1
Nrgn
Cd2
Ms4a4b
Prkch
Cx3cr1
Il2rb
Cd7
Tyrobp
Ifitm1
Slamf7
Fcer1g
Tbx21
Gzmb
Nkg7
Il18r1
Il7r
Id2
Il23r
Il1r1
Cd44
γδT1
γδT1p
γδTe1
γδTe2
αβT
γδT17pw
γδT17pk
γδT17
E
WT
HEB cKO
cells/cluster
750
600
450
300
150
0
3-αβT
2-γδTe1
6-γδTe2
4-γδT17pw
1-γδT17pk
5-γδT17
0-γδT1p
7-γδT1
F
Trpm1
Nr4a1
Bcl3
Ifi27l2a
Phf11b
Tagap
Nrgn
Eno3
Ephx1
Tnfrsf9
Klra5
Tyrobp
Ifitm1
Klrb1a
Scimp
Klrc1
Sh2d1b1
Klrc2
Car2
Gm156
Sox5
Slc15a1
Rab27b
4932438H23Rik
Ptgir
Sstr2
Wfs1
Etv5
Gm29017
Mpp4
Igfbp4
Tuba8
Ptpn14
Pgam2
Hivep3
Itm2a
Slc22a3
Eads2
Trim13
Dnph1
Cd8a
Cd8b1
Gm37065
Rag1
Rag2
Chrna9
H19
Dgkeos
Arpp21
Prss57
Clnk
Tns4
Socs2
Slc15a3
Adam8
Il23r
Ltb4r1
Serpinb1a
Il1r1
Itgb5
Fam83a
Grifin
Il17re
1700012B07Rik
Furin
Maf
Cpne8
Icos
Mzb1
Gm13652
Sdc4
Il17a
Nlrx1
5830411N06Rik
Wnt8b
Zbtb8b
Igch
Pde6a
Notch3
Nebl
γδTe1
γδTe2
αβT
γδT17pw
γδT17pk
γδT17
γδT1
γδT1p

Figure 3

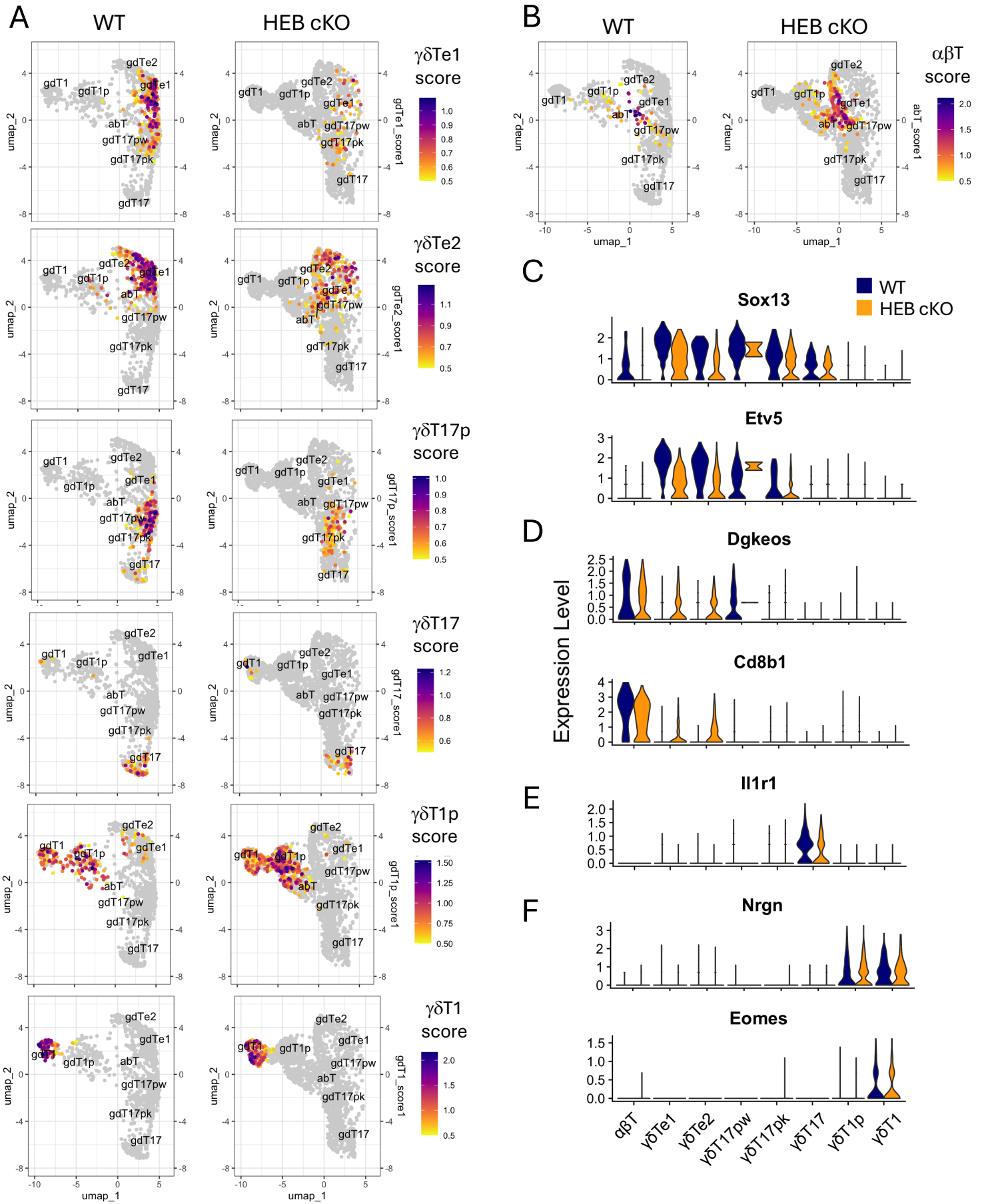
A
WT
HEB cKO
γδTe1 score
γδTe2 score
γδT17p score
γδT17 score
γδT1p score
γδT1 score
gdT1
gdT1p
gdTe1
gdTe2
abT
gdT17pw
gdT17pk
gdT17
umap_1
umap_2
B
αβT score
abT_score1
C
WT
HEB cKO
Sox13
Etv5
D
Dgkeos
Cd8b1
Expression Level
E
Il1r1
F
Nrgn
Eomes
αβT
γδTe1
γδTe2
γδT17pw
γδT17pk
γδT17
γδT1p
γδT1

Figure 4

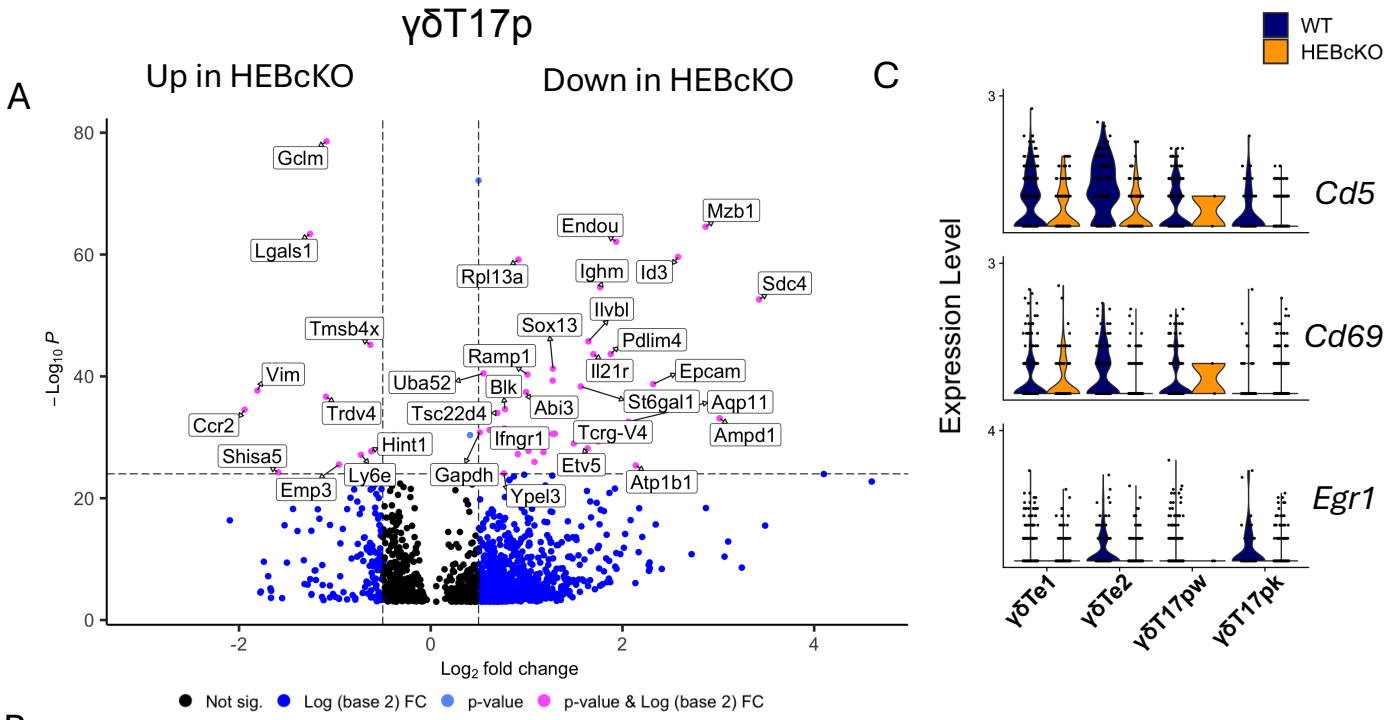

B

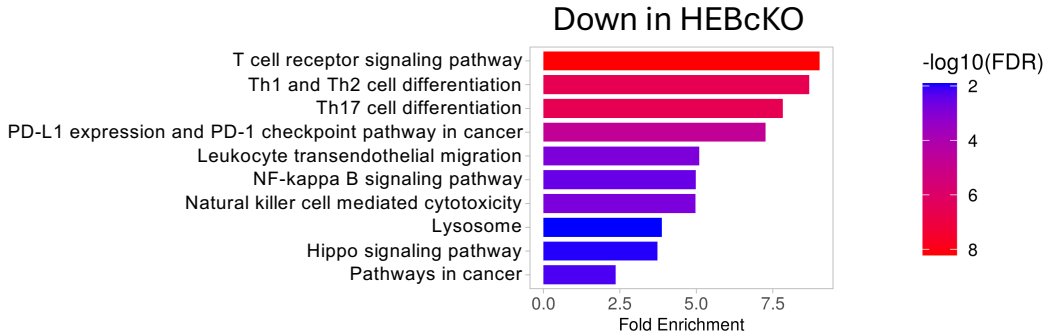

D

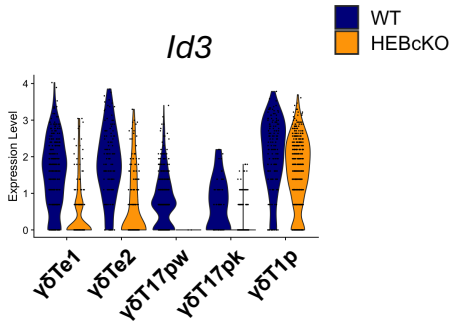

E

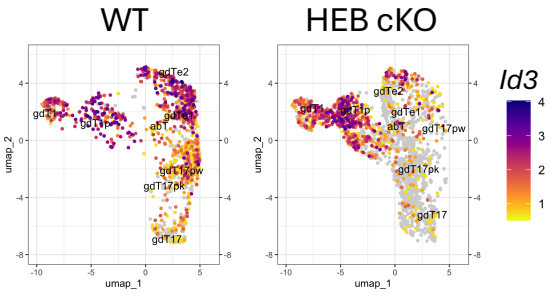

F

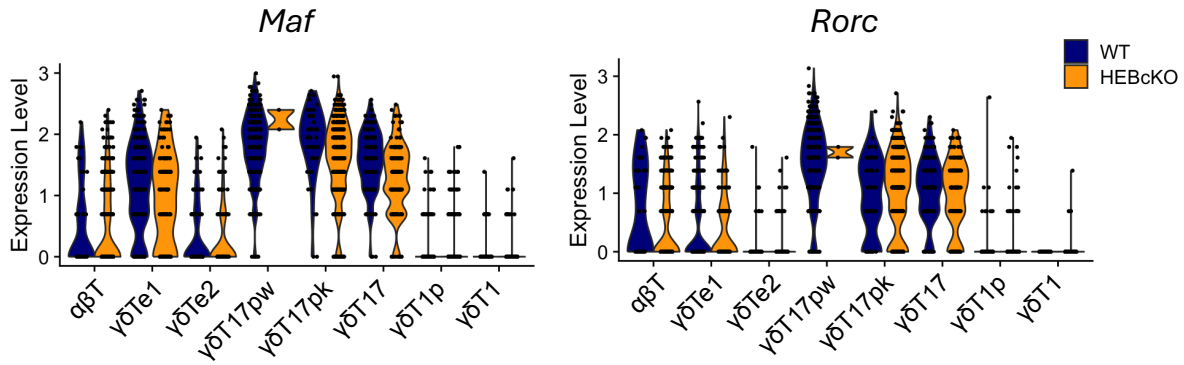

Figure 5

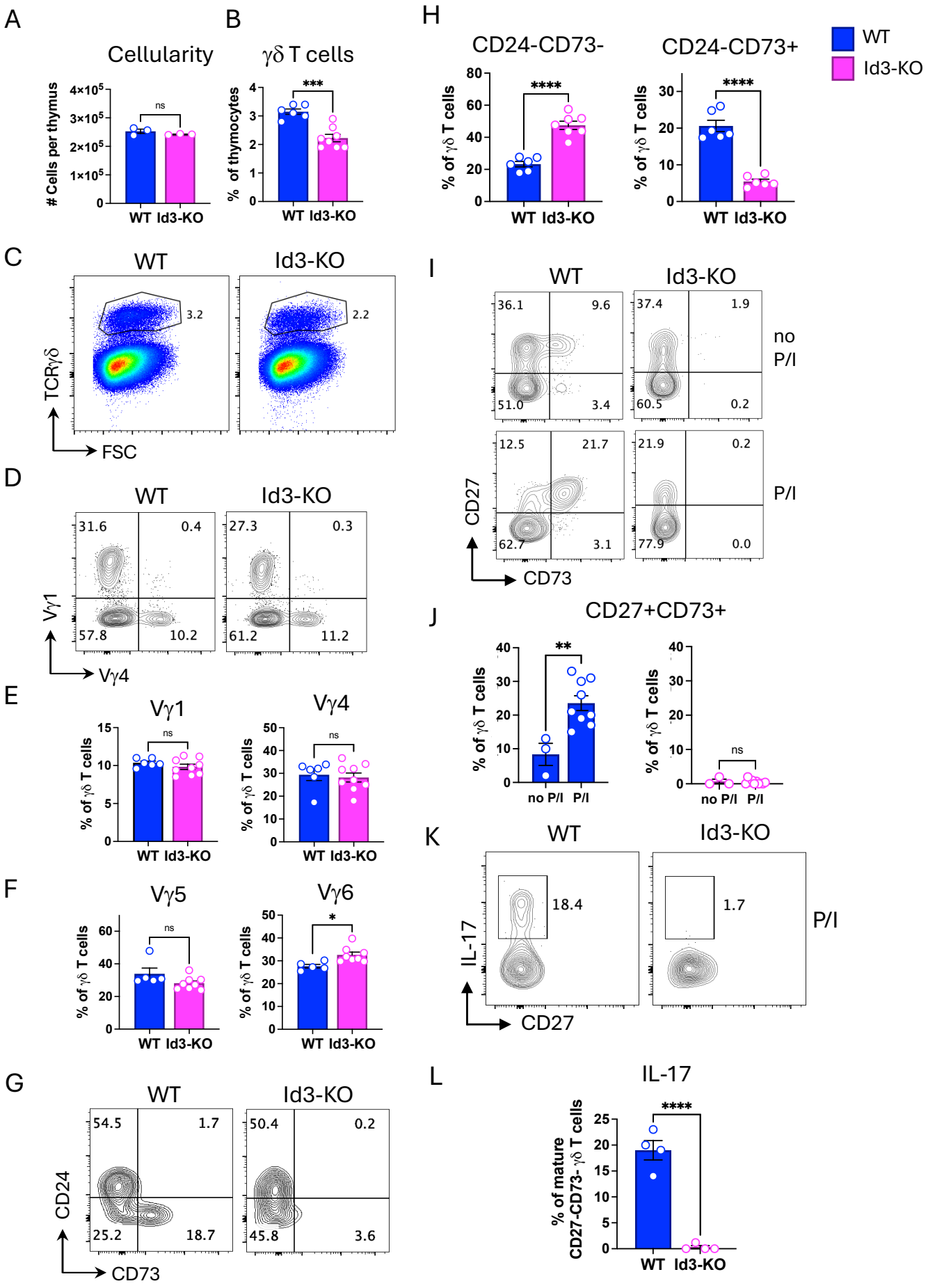
A
Cellularity
Cells per thymus
4×10^5
3×10^5
2×10^5
1×10^5
0
ns
WT Id3-KO
B
γδ T cells
% of thymocytes
***
WT Id3-KO
H
CD24-CD73-
CD24-CD73+
% of γδ T cells
****
WT Id3-KO
WT
Id3-KO
C
WT
Id3-KO
3.2
2.2
TCRγδ
FSC
D
WT
Id3-KO
31.6
0.4
57.8
10.2
27.3
0.3
61.2
11.2
Vγ1
Vγ4
E
Vγ1
Vγ4
% of γδ T cells
ns
WT Id3-KO
F
Vγ5
Vγ6
% of γδ T cells
ns
*
WT Id3-KO
G
WT
Id3-KO
54.5
1.7
25.2
18.7
50.4
0.2
45.8
3.6
CD24
CD73
I
WT
Id3-KO
36.1
9.6
51.0
3.4
37.4
1.9
60.5
0.2
no P/I
12.5
21.7
62.7
3.1
21.9
0.2
77.9
0.0
P/I
CD27
CD73
J
CD27+CD73+
% of γδ T cells
**
ns
no P/I
P/I
K
WT
Id3-KO
18.4
1.7
P/I
IL-17
CD27
L
IL-17
% of mature CD27-CD73- γδ T cells
****
WT Id3-KO

Figure 6

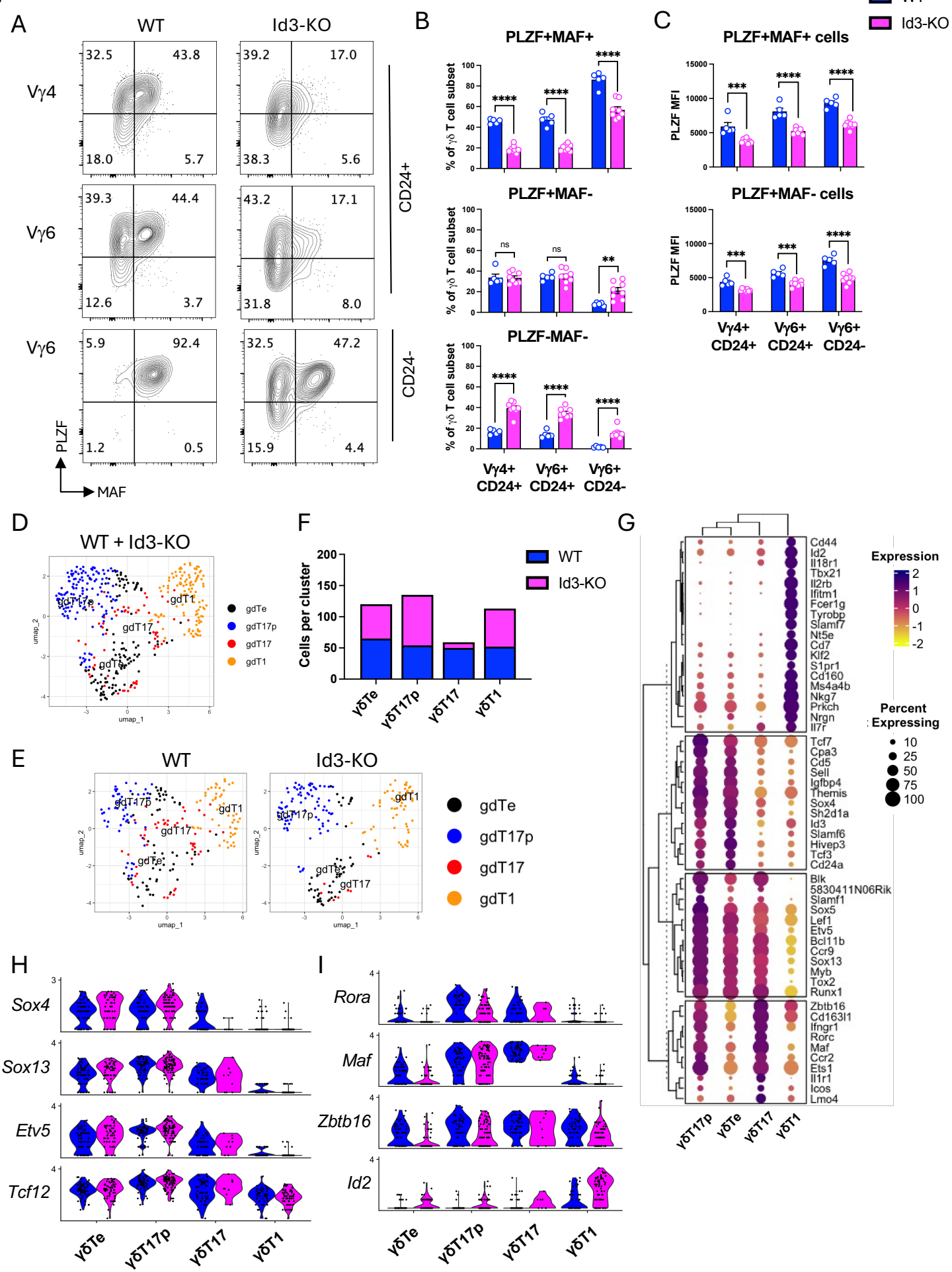
A
WT
Id3-KO
Vγ4
Vγ6
Vγ6
CD24+
CD24-
PLZF
MAF
32.5
43.8
18.0
5.7
39.2
17.0
38.3
5.6
39.3
44.4
12.6
3.7
43.2
17.1
31.8
8.0
5.9
92.4
1.2
0.5
32.5
47.2
15.9
4.4
B
PLZF+MAF+
PLZF+MAF-
PLZF-MAF-
% of γδ T cell subset
Vγ4+ CD24+
Vγ6+ CD24+
Vγ6+ CD24-
C
WT
Id3-KO
PLZF+MAF+ cells
PLZF+MAF- cells
PLZF MFI
D
WT + Id3-KO
gdTe
gdT17p
gdT17
gdT1
umap_1
umap_2
E
WT
Id3-KO
F
Cells per cluster
γδTe
γδT17p
γδT17
γδT1
G
Expression
Percent Expressing
Cd44
Id2
Il18r1
Tbx21
Il2rb
Ifitm1
Fcer1g
Tyrobp
Slamf7
Nt5e
Cd7
Klf2
S1pr1
Cd160
Ms4a4b
Nkg7
Prkch
Nrgn
Il7r
Tcf7
Cpa3
Cd5
Sell
Igfbp4
Themis
Sox4
Sh2d1a
Id3
Slamf6
Hivep3
Tcf3
Cd24a
Blk
5830411N06Rik
Slamf1
Sox5
Lef1
Etv5
Bcl11b
Ccr9
Sox13
Myb
Tox2
Runx1
Zbtb16
Cd163l1
Ifngr1
Rorc
Maf
Ccr2
Ets1
Il1r1
Icos
Lmo4
H
Sox4
Sox13
Etv5
Tcf12
I
Rora
Maf
Zbtb16
Id2

Figure 7

A

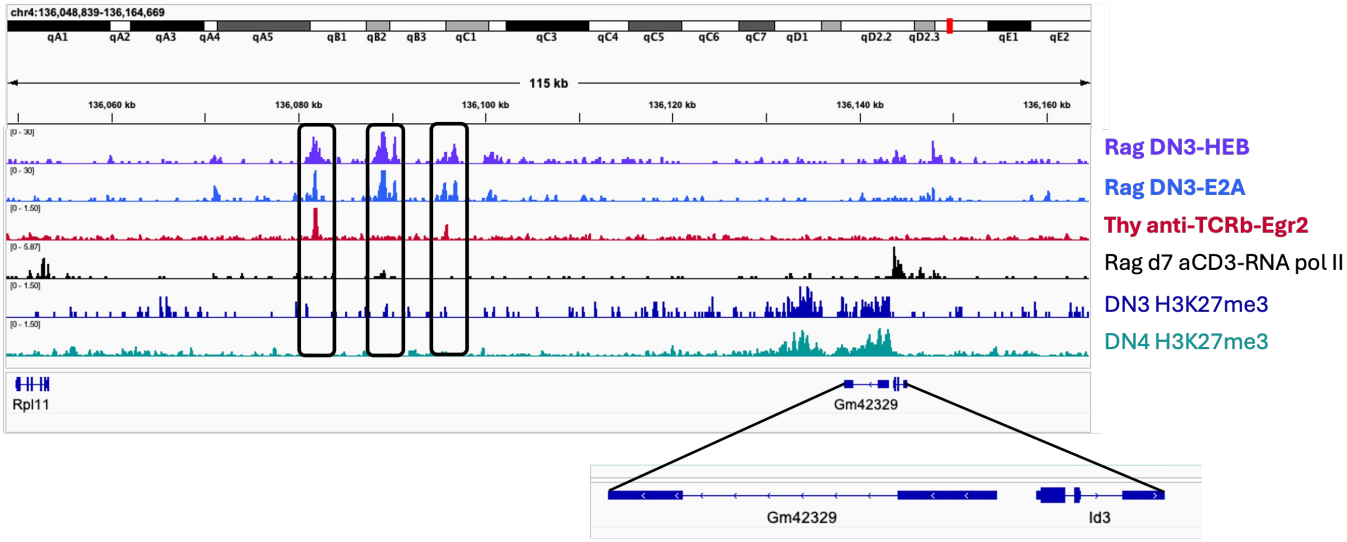

B

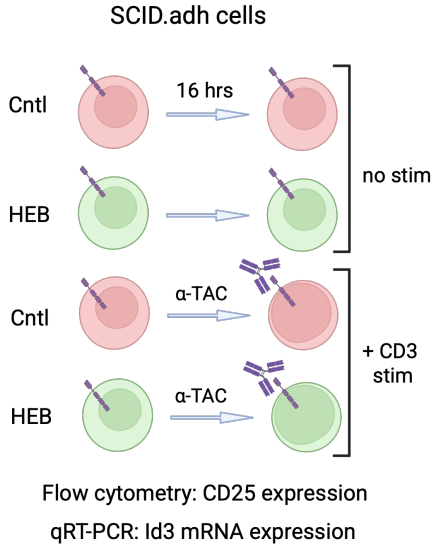

C

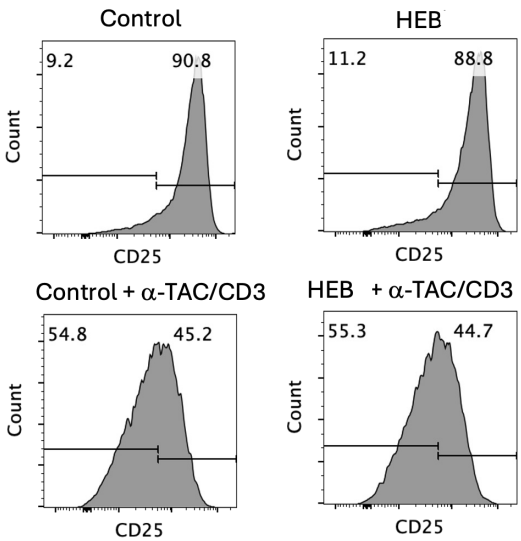

D

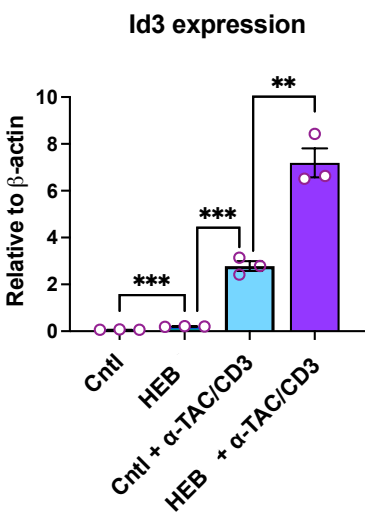

E

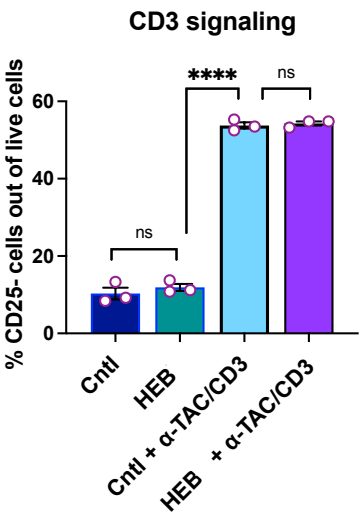

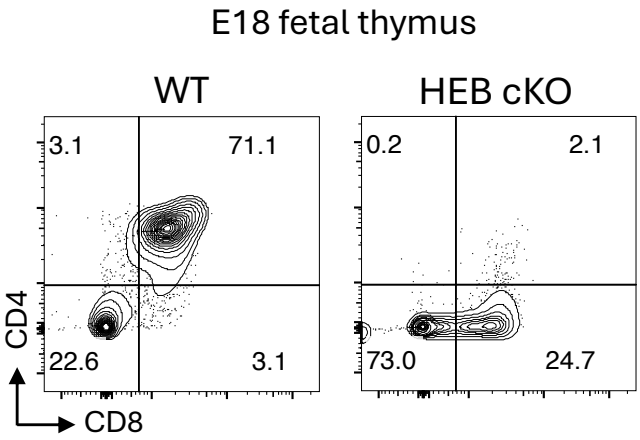

Supplementary Figure 1. Defects in αβ T cell development in E18 fetal thymus of HEB cKO mice. Thymocytes were dissected from E18 WT and HEB cKO littermates and subjected to flow cytometry. At E18 very few cells had become CD4 or CD8 single positives with most cells at the DP stage in WT mice. The DN to ISP and ISP to DP transitions were severely compromised in the HEB cKO fetal thymus, in agreement with the previously reports of HEB-deficient adult mice.

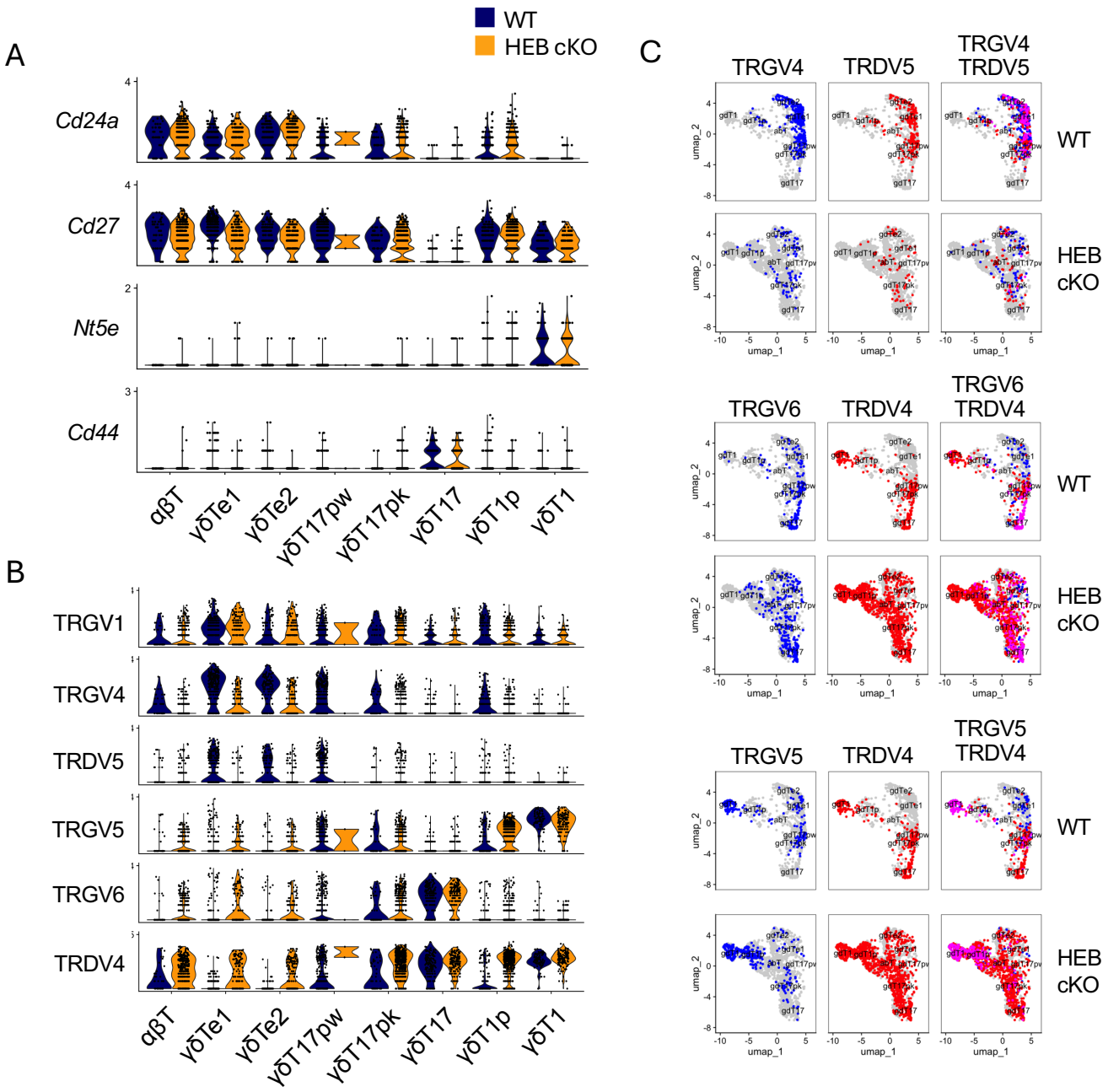

Supplementary Figure 2. TRGV and TRDV expression profiling reveals depletion of TRDV4 and TRDV5 transcripts and overexpression TRDV4 in the HEB cKO fetal γδ T cells. **A**. Violin plots of expression of canonical genes that mark γδ T cell subsets. **B**. Violin plots showing expression of TRGV and TRDV genes in WT versus HEB cKO by cluster. WT = blue, HEB cKO = orange. **C**. Blended split feature plots showing cells expressing TRGV chains (blue) or TRDV chains (red), and cells co-expressing TRGV and TRDV chains (pink). Co-expression in WT cells are shown on the top panel of each comparison and HEB cKO cells are shown on the bottom.

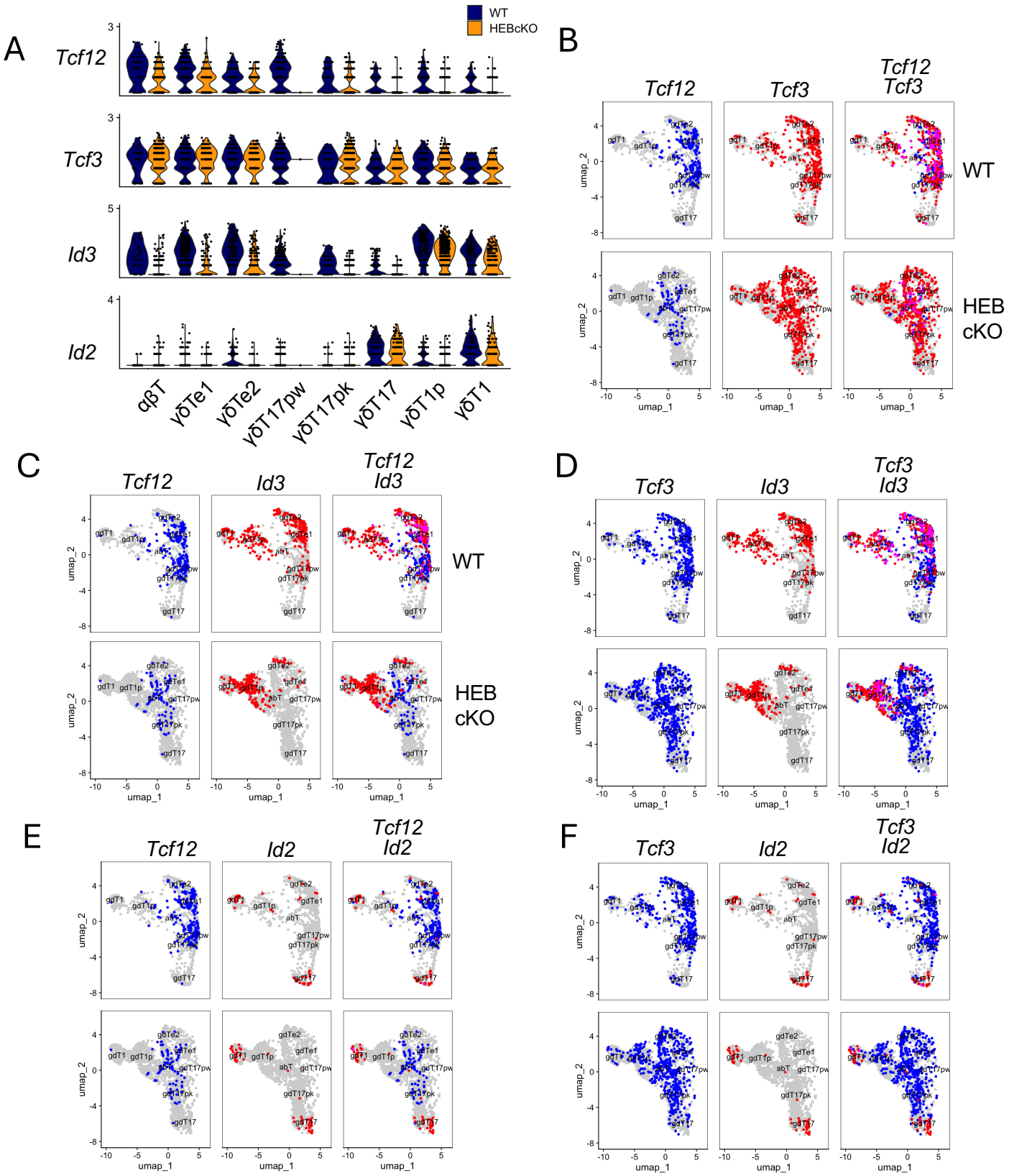

Supplementary Figure 3. Patterns of E protein and Id protein gene expression during γδ T cell development in WT and HEB cKO mice. A. Relative expression of *Tcf12* (HEB), *Tcf3* (E2A), *Id3*, and *Id2* in WT versus HEB cKO cells by cluster. WT = blue, HEB cKO = orange. C-F. Co-expression of E protein and Id protein transcripts assessed by blended split feature plots, for (B) *Tcf12* and *Tcf3*, (C) *Tcf12* and *Id3*, (D) *Tcf3* and *Id3*, (E) *Tcf12* and *Id2*, and (F) *Tcf3* and *Id2*. Blue = E protein gene expression, red = Id gene expression, pink = co-expression.

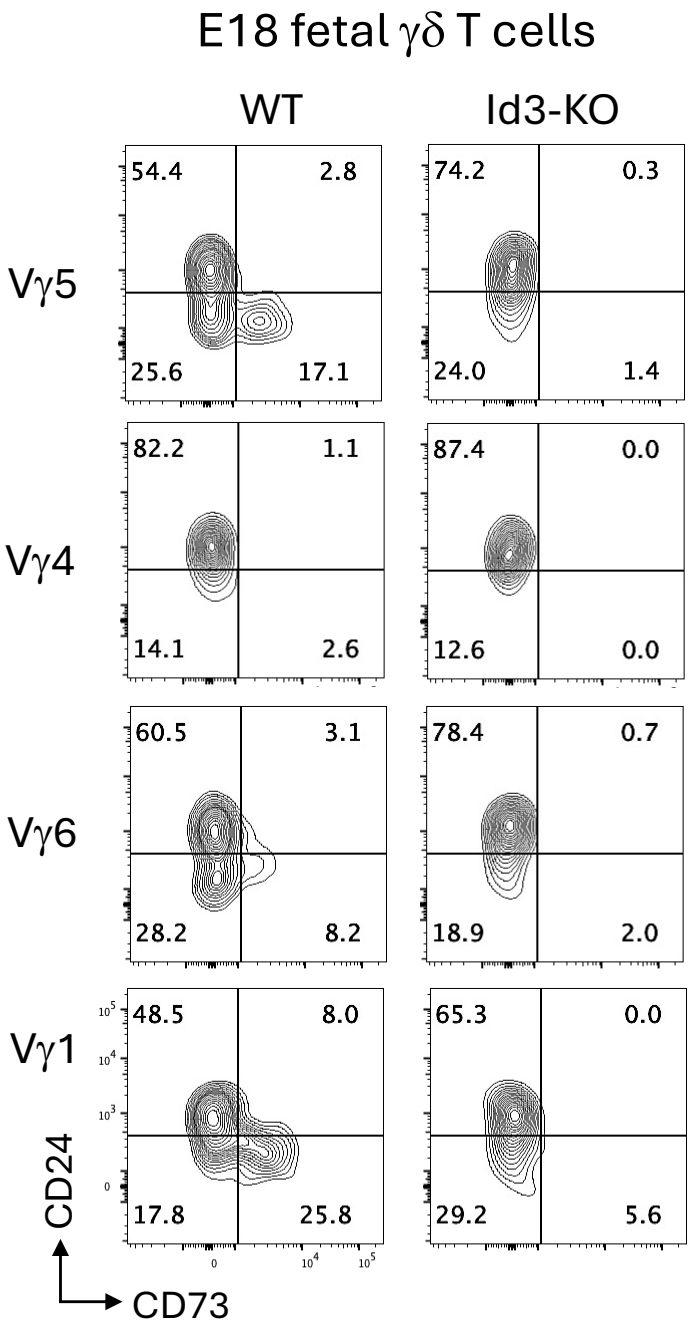

Supplementary Figure 4. CD73 is upregulated during development of Vγ5 and Vγ1 γδ T cells in WT but not Id3-KO fetal thymus. Flow cytometry plots of CD24 and CD73 expression within the Vγ subsets from WT and Id3-KO E18 fetal thymus.

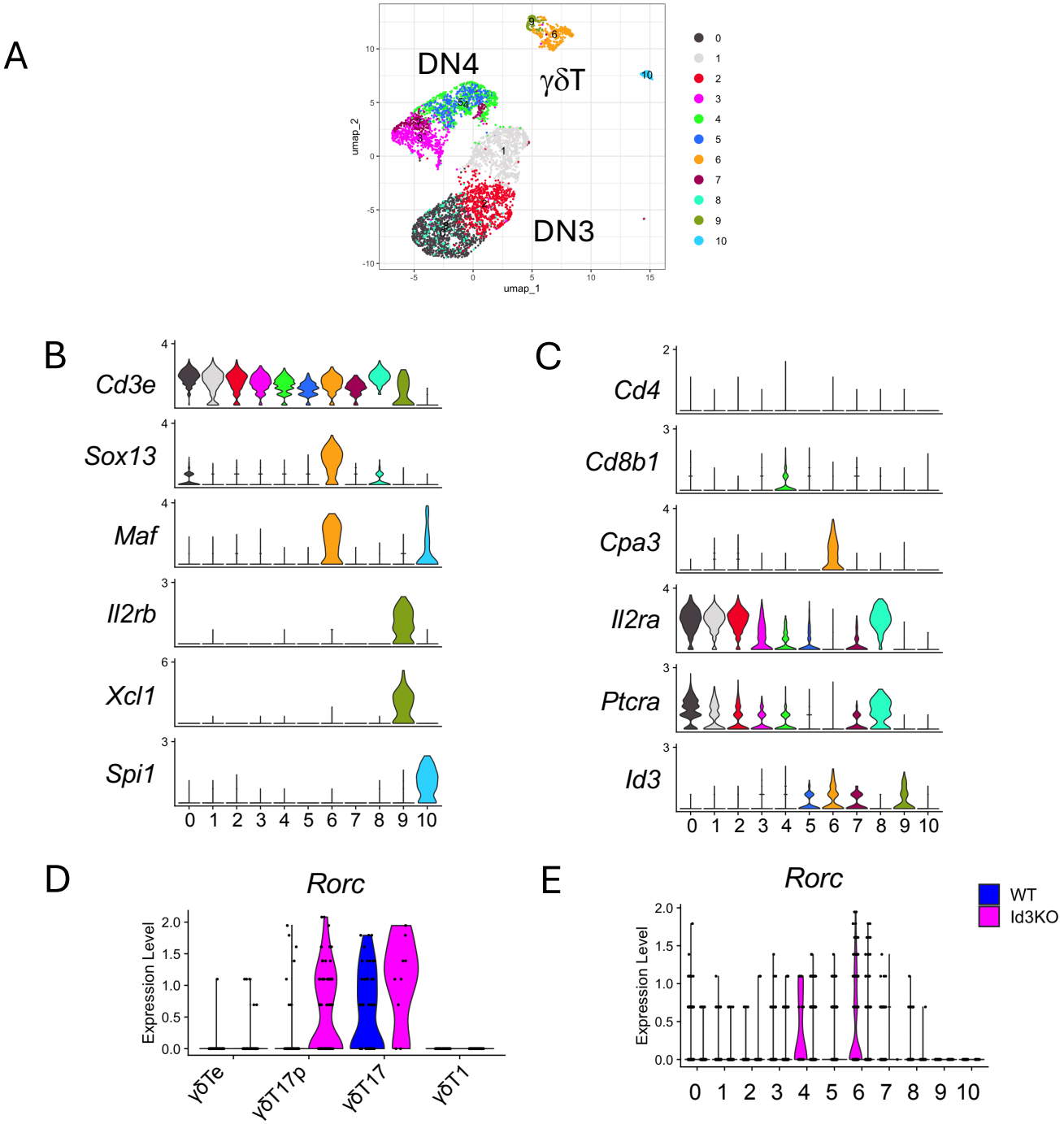

Supplementary Figure 5. Identification of γδ T cell subsets from E18 WT and Id3-KO DN cells using scRNA-seq. WT and Id3-KO E18 thymocytes were pooled and subjected to magnetic sorting to obtain CD4$^-$CD8$^-$ (DN) cells for scRNA-seq. A. UMAP of merged dataset depicting 11 clusters (0-10). B. Expression of lineage-defining genes to assign identities to clusters in merged dataset: *Cd3e* for T-lineage, *Spi1* (encodes PU.1) for myeloid lineage, *Sox13* for γδT17 lineage, *Maf* for myeloid and γδT17 lineages, and *Il2rb* and *Xcl1* for γδT1 lineage. C. Expression of genes defining DN subsets in merged datasets: *Cpa3* for DN2 and γδ T cells, *Il2ra* (encodes CD25) for DN2/3 cells, *Ptcra* (encodes pre-Tα) for DN3 cells, and *Id3* for γδ T cells and DN4 cells. *Cd8b1* is upregulated transcriptionally before surface expression and marks αβ-T lineage commitment within DN4 cells. *Cd4* was undetectable, validating our MACS enrichment strategy. D. Expression of *Rorc* in WT versus Id3-KO cells in γδ T cell subsets. E. *Rorc* expression in all WT and Id3-KO clusters.

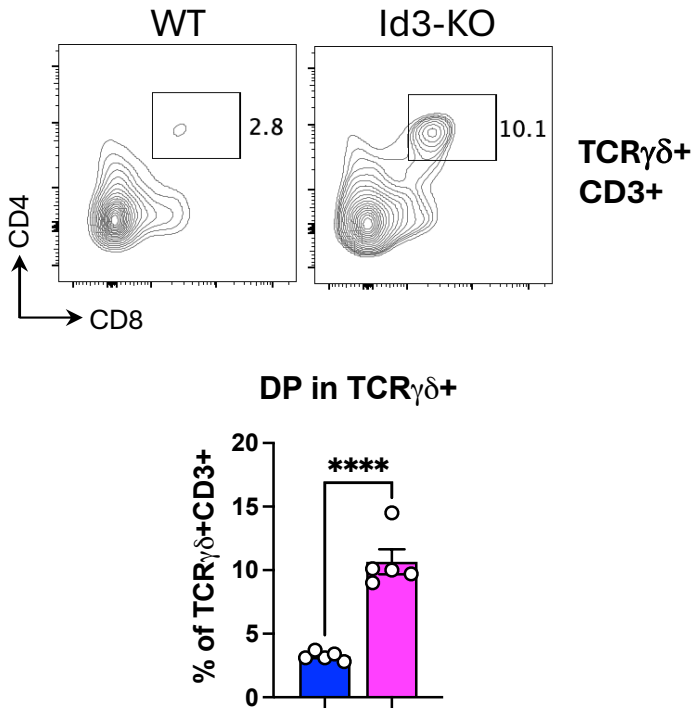

Supplementary Figure 6. γδTCR$^+$ cells from E18 Id3-KO mice include a population of CD4$^+$CD8$^+$ cells, indicating diversion to the αβ-T lineage program. E18 fetal thymocytes were subjected to flow cytometry. Cells were gated on the TCRγδ$^+$CD3+ population and analyzed for expression of CD4 and CD8 which was quantified in a bar graph depicting the percentage of CD4$^+$CD8$^+$ (DP) cells within the γδTCR$^+$ population.

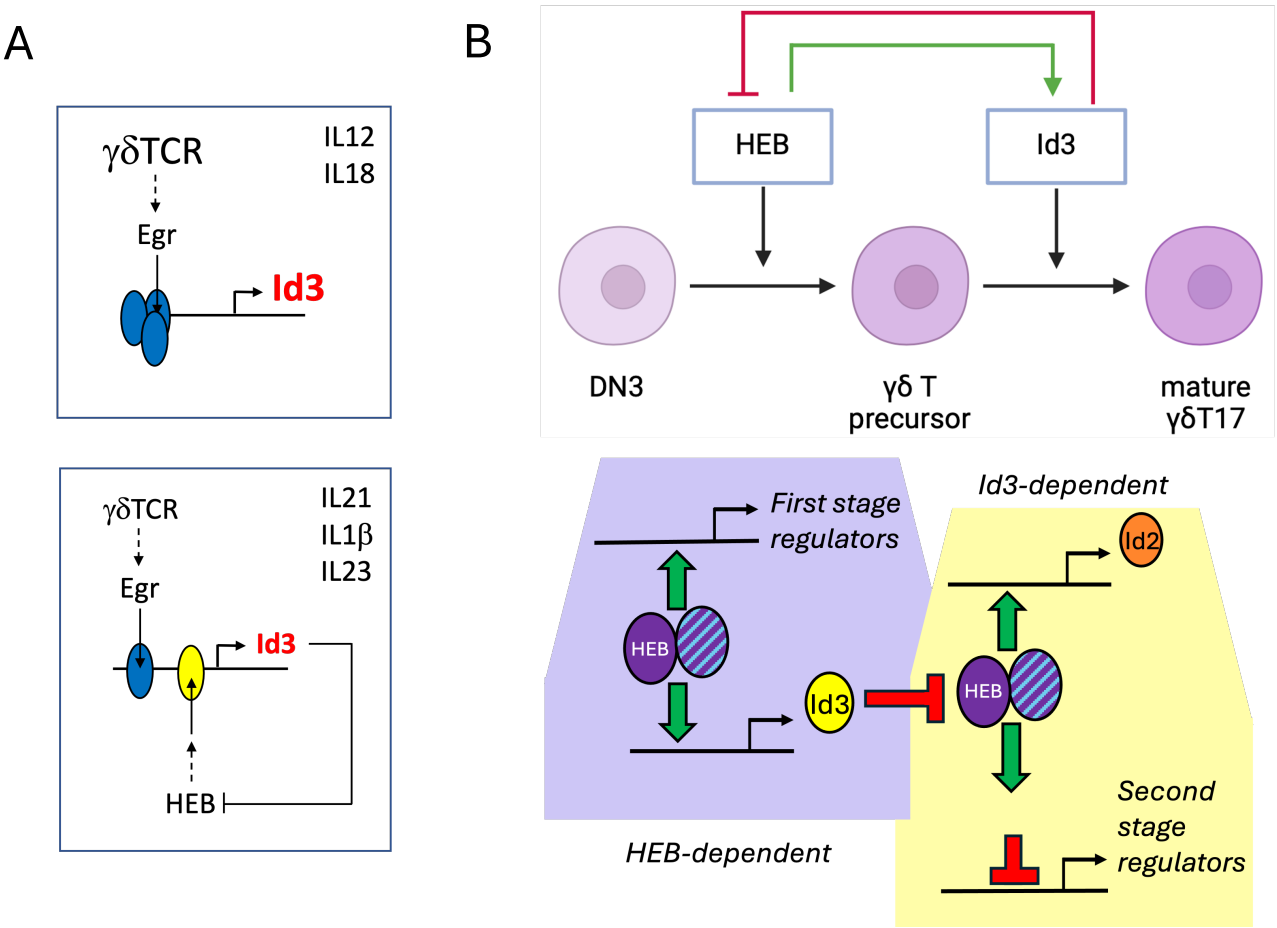

Supplementary Figure 7. Model for HEB and Id3 requirements in the development and maturation of γδT17 cells. A. Strong γδTCR signaling induces high levels of Egr2, which are sufficient to drive Id3 upregulation without HEB, whereas HEB is also required under lower γδTCR signaling conditions. Distinct cytokine signals also participate in *Id3* modulation and γδ T cell lineage choice. **B**. γδT17 development occurs in two stages, the first of which is HEB-dependent, and the second of which is Id3-dependent. HEB induces Id3 during the first stage, which acts in a negative feedback loop to inhibit HEB activity during the second stage. The absence of *Id3* allows higher E protein activity, which inhibits second stage regulators but also results in *Id2* upregulation, providing partial compensation for the loss of *Id3*.